CHALMERS
UNIVERSITY OF TECHNOLOGY

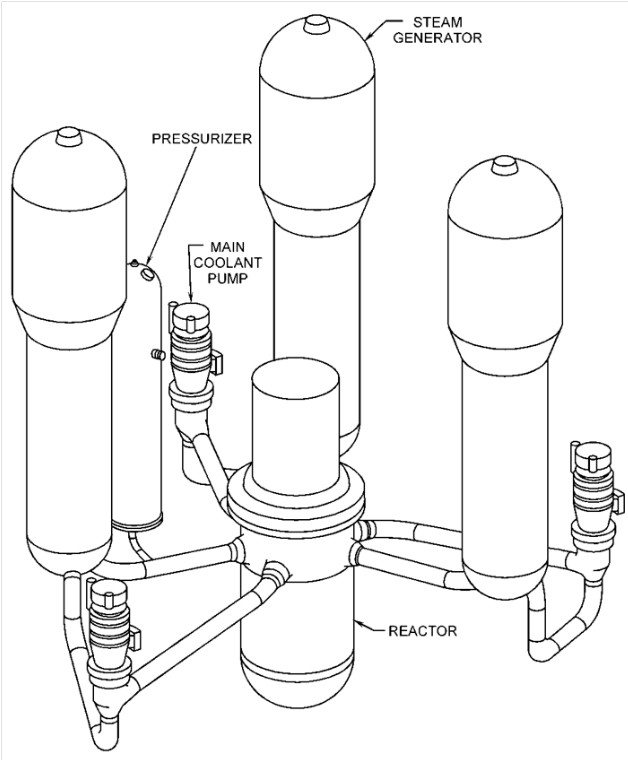

Analysis of a Load Step Test at Ringhals 4 NPP using RELAP5 Code

Model Validation and Verification

Master's Thesis in Nuclear Science and Technology

ATHANASIOS STATHIS

Department of Applied Physics
CHALMERS UNIVERSITY OF TECHNOLOGY
Gothenburg, Sweden 2015

Master's thesis 2015:NN

Analysis of a Load Step Test at Ringhals 4 NPP Using RELAP5 Code

Model Validation and Verification

ATHANASIOS STATHIS

CHALMERS
UNIVERSITY OF TECHNOLOGY

Department of Applied Physics
Division of Nuclear Engineering
Chalmers University of Technology
Gothenburg, Sweden 2015

Analysis of a Load Step Test at Ringhals 4 NPP using RELAP5 Code.
Model Validation and Verification.
ATHANASIOS STATHIS

Supervisor: Dr. Jozsef Bánáti, Department of Applied Physics
Examiner: Assoc. Prof. Anders Nordlund, Department of Applied Physics

Master's Thesis 2015:NN
Department of Applied Physics
Division of Nuclear Engineering
Chalmers University of Technology
SE-412 96 Gothenburg
Telephone +46 31 772 1000

Cover: 3-loop Westinghouse Pressurised Water Reactor [5].

Typeset in LaTeX
Printed by [Name of printing company]
Gothenburg, Sweden 2015

Analysis of a Load Step Test at Ringhals 4 NPP Using RELAP5 Code.
Model Validation and Verification.
ATHANASIOS STATHIS
Department of Applied Physics
Chalmers University of Technology

Abstract

Ringhals 4 unit, a Westinghouse deign Pressurized Water Reactor, has recently undergone a pressurizer and steam generator replacement. In March 2015 the reactor was licenced to operate at the uprated 3300 MW_{th} nominal thermal power level. Load Step Test is among the first tests performed in the reactor at the uprated power conditions.

During the Load Step Test, while the reactor is in steady state, the turbine power is sharply reduced by 10 %. Fast insertion of the control rods follows and the reactor is stabilized in an intermediate steady state. After 3000 s in the intermediate steady state the control rods are quickly withdrawn in order to sharply increase the turbine power by 10 % and restore the reactor to its nominal steady state.

The purpose of the Load Step Test is to verify that the control systems can mitigate the transient. The data from this test can be used for the assessment and improvement of RELAP5 model of Ringhals 4. Validation of the model was performed by the simulation of the transient.

Thus, the first step is that the code reaches a realistic steady state close to the one of the plant in the beginning of the test. This task is accomplished. The challenges occurred during this stage are mentioned as well the way they were tackled. In addition, strategies for achieving steady state are touched upon.

The next step is the simulation of the whole transient. The process/way of thinking that led to specific improvements in the model is described, as well as the key parameters for the further improvement of the model.

In the end, the "goodness" of the improved model is assessed using the Fast Fourier Transformed Method (FFTBM). FFTBM proves that the model is capable of predicting the transient quite accurately.

Keywords: Fast Fourier Transform Based Method (FFTBM), Load Step Test, RELAP5, Ringhals 4, Transient.

Acknowledgements

I would like to express my deep gratitude to my beloved parents, Kaloudis and Irini, and to my beloved brother Vasilis. Thank you for supporting me during my master studies despite the financial confinements imposed by the Greek financial crisis. Thank you very much for your trust and your encouragement. I wouldn't make it without you. I devote this thesis to you. I send you my love and my best wishes to each one to you personally.

I would also like to thank my supervisor, Dr. Jozsef Bánáti for his vital support and help during this thesis project. I am very glad to cooperate with such an exceptional man. As a supervisor he was very inspiring and kindly offered me the chance to become co-author in one his scientific reports. I have benefited a lot from his engineering thinking. I appreciate him a lot and I will definitely miss the nice discussions we had during our sessions.

Moreover, I would like to thank my industry counsellor, Marie Hagman, for her kind support and her encouragement as well as for her valuable advices.

I also feel thankful for Dr. Andrej Prošek for his valuable contribution to my master thesis project. Dr. Prošek kindly answered my questions about FFTBM, providing the programme being used for the FFTBM calculations as well as papers and publications about FFTBM issues.

Special thanks my opponents, Karin Warholm and Roger Hurtig for their comments, as well as my examiner Dr. Anders Nordlund for supporting my participation in RELAP5 meetings along with my supervisor.

And last but not least, I would like to send my warm regards to Dr. Nikos Petropoulos from Athens. He is the man who taught me the first course in Nuclear Engineering and who inspired me to follow this discipline.

Athanasios Stathis, Gothenburg, November 2015

Contents

List of Figures

List of Tables

Abbreviations

AA	Average Amplitude
AA_{tot}	Total Average Amplitude
BE	Best Estimate
BWR	Boiling Water Reactor
$CVCS$	Chemical and Volume Control System
DFT	Discrete Fourier Transformation
FFT	Fast Fourier Transformation
$FFTBM$	Fast Fourier Transform Based Method
$LOCA$	Loss of Coolant Accident
LWR	Light Water Reactor
MCP	Main Circulation Pump
ND	Number of Discrepancies
$PHWR$	Pressurized Heavy Water Reactor
$PORV$	Power Operated Relief Valve
PRZ	Pressurizer
PWR	Pressurized Water Reactor
$RHRS$	Residual Heat Removal System
RPV	Reactor Pressure Vessel
$SB-LOCA$	Small Break Loss of Coolant Accident
$SCRAM$	Safety Control Rods Activator Mechanism
SG	Steam Generator
VA	Variable Accuracy
VA_{max}	Maximum Variable Accuracy
VA_{min}	Minimum Variable Accuracy

1 Introduction

Nuclear Power is a source of energy used as base load with minimum CO_2 emissions. The power density of a nuclear power plant produces by far more power than the conventional and renewable power sources (e.g. wind mills farms, solar panels farm). Nuclear power is also considered cheap as the lifetime of an ordinary plant can be extended to operate around 60 years and the basis. The fuel, uranium, is cheap and its price does not fluctuate significantly.

Uranium price is very unlikely to vary significantly due to political reasons. It is worth mentioning that the fuel used in most of the light water reactors (LWRs) is enriched around 3-3.5 % ^{235}U. ^{235}U is the isotope that contributes to the energy output of the fuel. Thus, there is a huge margin of improvement in fuel efficiency.

Despite the above favorable characteristics of nuclear power public opinion in many countries is very sceptic about its adoption, mainly due to safety concerns. Chernobyl and Fukushima accidents have damaged a lot the reputation of nuclear energy.

However the safety of the current third generation reactors has massively improved the last decades and nuclear energy is considered a safe energy source. A huge effort has been put on the mitigation and prediction/simulation of the most important class of accidents, the loss of coolant accidents (LOCAs) using small scaled facilities of commercial prototype reactors. In addition, tests are performed in the reactors themselves in order to verify the ability of the control systems to mitigate deviations from ordinary operation conditions. Among those maneuverability tests, the Load Rejection [6], SCRAM Test and the Load Step Test [7, 4] are the most important. The complexity and the time required for its analysis make the Load Step Test very suitable for a master thesis project. This master thesis deals with the analysis of the Load Step Test performed in 2015-03-03 in Ringhals 4 unit.

1.1 Nuclear Energy in Sweden

Nuclear energy in Sweden accounts for 41.47 % of the total electricity production in the country just behind hydro-power electricity production which accounts for around 45 % of the total electricity production.

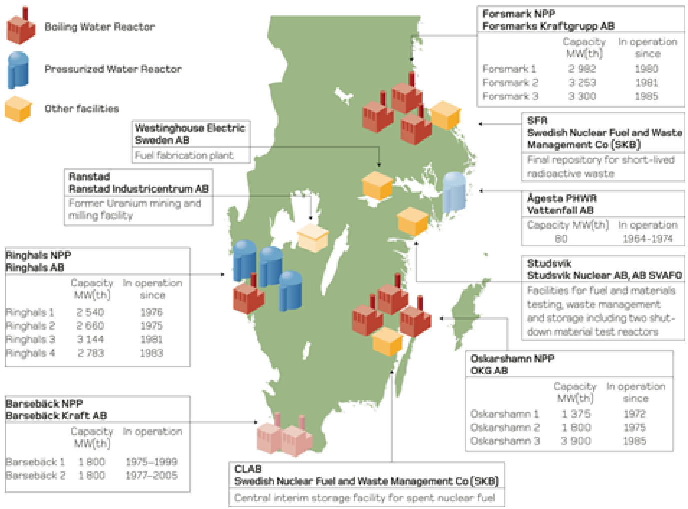

Figure 1.1: Nuclear reactors of Sweden [30].

The first reactor to be critical in Sweden was a Pressurized Heavy Water Reactor (PHWR) in Ågesta in 1964. This reactor had a power output of 10 MW_e and was used mainly for district heating of the wider Stockholm region. However, it produced a small amount of electricity also. Ågesta reactor operated for 10 years, until 1974 when it was permanently shut down.

The first commercial reactor commissioned was Oskarshamn 1 Boiling Water Reactor (BWR) in 1972. Until 1980 another 9 units were commissioned in the sites of Oskarshamn, Ringhals, Forsmark and Barsebäck.

In the aftermath of Three-Mile-Island accident a referendum was held in Sweden concerning the future of nuclear energy in the country. The outcome of the referendum was to continue with the construction of Ringhals 3 and 4 units and that the reactor of operating units would be 12. In addition the safety systems of Barsebäck 3 unit had to be improved. It was also decided that all the units should be phased out until 2010.

With the occurrence Chernobyl accident in 1985, a new legislation had been ratified in 1987 by the parliament which prohibited the construction of new units. However, in a poll held in 2001 the Swedish people seemed to have a very positive attitude towards nuclear. 76 % voted for the continuation of nuclear industry.

In 2010 the legislation was modified to allow for improvements in the operating units. Life extension for most of the units was granted and investments were headed towards improving the operated units.

Finally, in 2014 the government has ceased any initiatives for building new units and the country is heading towards to the complete phase out of its nuclear power plants in the foreseeable future.

During 2015 Oskarshamn 2 unit phased out and Oskarshamn 1 unit along with Ringhals units 1 and 2 are also expected to stop electricity production by 2020. Barsebäck units 1 and 2 were phased out in 1999 and 2005 respectively.

Reactor Unit	*Type*	*Status*	*Operator*	*Gross Capacity (MW_e)*	*Commercial Operation*	*Decommissioning*
Forshmark-1	BWR	Operational	Vattenfall	1022	1980	2040
Forshmark-2	BWR	Operational	Vattenfall	1158	1981	2041
Forshmark-3	BWR	Operational	Vattenfall	1212	1985	2045
Oskarshamn-1	BWR	Operational	OKG	492	1972	2017-19
Oskarshamn-2	BWR	Operational	OKG	661	1974	2015
Oskarshamn-3	BWR	Operational	OKG	1450	1985	2035 or 2045
Ringhals-1	BWR	Operational	Vattenfall	910	1976	2020
Ringhals-2	PWR	Operational	Vattenfall	847	1975	2019
Ringhals-3	PWR	Operational	Vattenfall	1117	1981	2041
Ringhals-4	PWR	Operational	Vattenfall	1168	1983	2043
Ågesta	PHWR	Shutdown	Barsebäck Kraft AB	12	1964	1974
Barsebäck-1	BWR	Shutdown	Barsebäck Kraft AB	615	1975	1999
Barsebäck-2	BWR	Shutdown	Barsebäck Kraft AB	615	1977	2005

Table 1.1: Data about the nuclear reactors in Sweden.

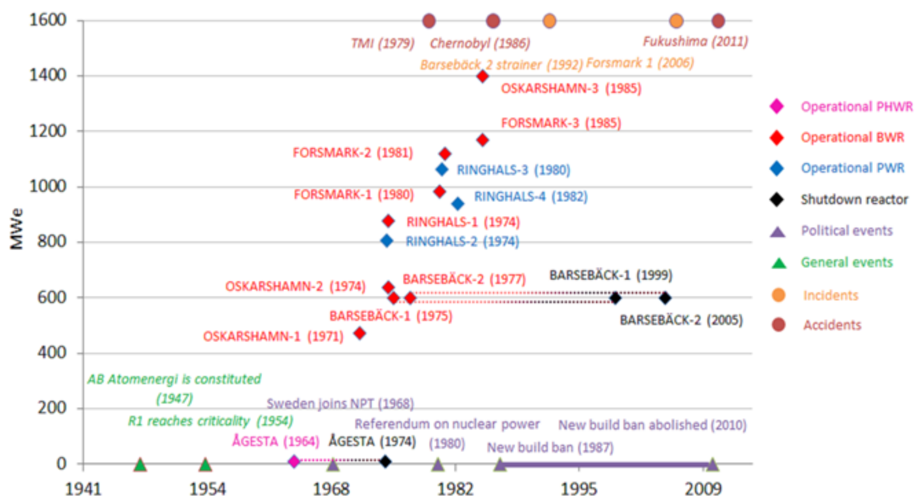

Figure 1.2: Timeline of nuclear reactors of Sweden [32].

1.2 Description of LWRs

Light Water Reactors (LWRs) are reactors that use water both as moderator and coolant. Two designs for LWRs exist. The Pressurized Water Reactor (PWR) and the Boiling Water Reactor (BWR). These types of reactors use Uranium as nuclear fuel usually 3 % enriched in U^{235} (the rest comprises of ^{238}U atoms). Thermal energy comes primarily from the fission of ^{235}U.

A fission reaction of ^{235}U occurs when a slowed down neutron/thermal neutron is absorbed by an ^{235}U nucleus. This reaction yields two or three fast neutrons along with two medium-heavy nuclei and the release of $200MeV$ energy. These fast neutrons need to be slowed down/moderated so as to be absorbed by other ^{235}U nuclei. Fast neutrons loose most of their kinetic energy by colliding with water molecules (water used as moderator).

Successive fissioning of ^{235}U leads in a chain reaction and increasing energy output which is controlled by the use of neutron absorbers. In PWRs diluted boron in water and control rods entering from the bottom of the reactor are used as neutron absorbers.

Thermal energy is also produced by fissioning of ^{238}U by fast neutrons and by fissioning of ^{236}U and ^{239}Pu. The two last isotopes are formatted by some of the successive decays of ^{238}U when it absorbs fast neutrons.

The fission energy produced is removed by turbulent water passing through channels in the fuel rods to be further utilised for electricity production and for cooling the fuel rods (water used as coolant).

1.3 Pressurized Water Reactor (PWR)

A PWR consist of two circuits, the primary and the secondary. The primary circuit includes the core the pressurizer (PRZ) and the primary side of the steam generator (SG) and the main circulation pumps (MCP). The secondary circuit includes the secondary side of the SG as well as the turbines and the condenser.

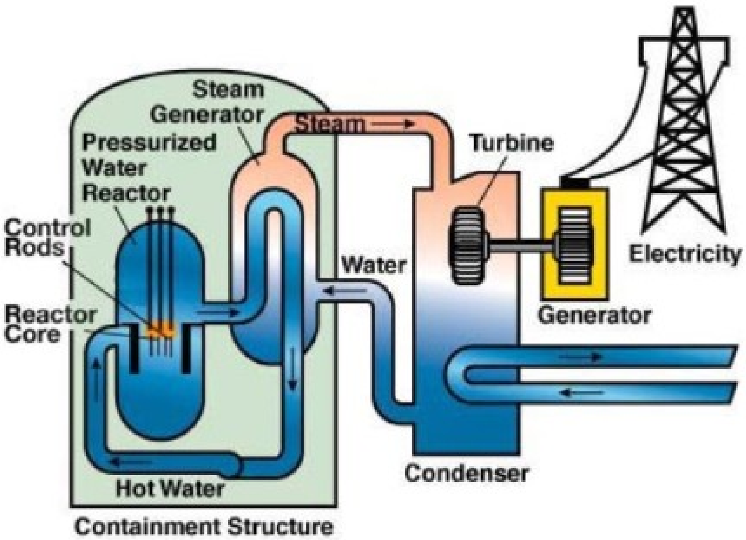

Figure 1.3: PWR outline [31].

The SG acts as heat exchanger between the primary and the secondary circuits whereas the PRZ is used for the regulation of the primary pressure.

Energy produced by fission reactions in the core heats the water in the primary side. The heated water passes from the SG where heat exchange occurs with the relatively cooler water of the secondary side of the SG. Hence, the heated water cools down and recirculates in the primary circuit.

The water in the cold side of the SG receives the heat of the water in the primary circuit and steam is produced. The steam is headed to the high and low pressure turbines and electricity is produced. After the passage from the turbines, condensers are used to condense the steam which is then recirculated in the secondary circuit.

A brief description of the PRZ and of a SG takes place in the following subsections.

1.3.1 The Pressurizer (PRZ)

The PRZ (figure 1.4) is a tank which contains water in its lower part and steam in the upper part, and is used to regulate the pressure in the primary circuit. In the upper part the PRZ is connected to a power operated relief valve (PORV) and a spray nozzle, whereas in the bottom part it is equiped with proportional and ON-OFF heaters.

The purpose of the PORV and of the spray nozzle is to relieve the pressure increase in the primary side. PORV achieves that by letting steam to be blown down through it. The spray nozzle achieves pressure relief by spraying water which condenses an amount of steam. Yet, there is always a constant small amount of spraying in steady state conditions in order to minimize the probability of their blockage in case of a transient condition.

On the other hand ON-OFF and proportional heaters (both pressure actuated) are used to increase the pressure. Both kind of heaters increase the pressure in the PRZ by expanding the water through heating. Proportional heaters are actuated in case of large pressure drops and they function always at full capacity. They are used to compensate smaller pressure drops and their capacity is analogous with the pressure deviation from the nominal value.

Figure 1.4: A Pressurizer (PRZ) [5].

1.3.2 The Steam Generator

The SG (figure 1.5) is a tank filled with water which is penetrated by primary side tubes of U-shape. Water of the SG in the vicinity of U-tubes lies at smaller pressure and temperature than the water flowing through them. As a result heat transfer occurs and the water around the U-tubes starts boiling. This lower section of the SG where boiling occurs is referred to as evaporation section. The wet steam produced in the evaporator passes in the steam drum section where wet steam is dried in steam separators before it is headed in the turbines.

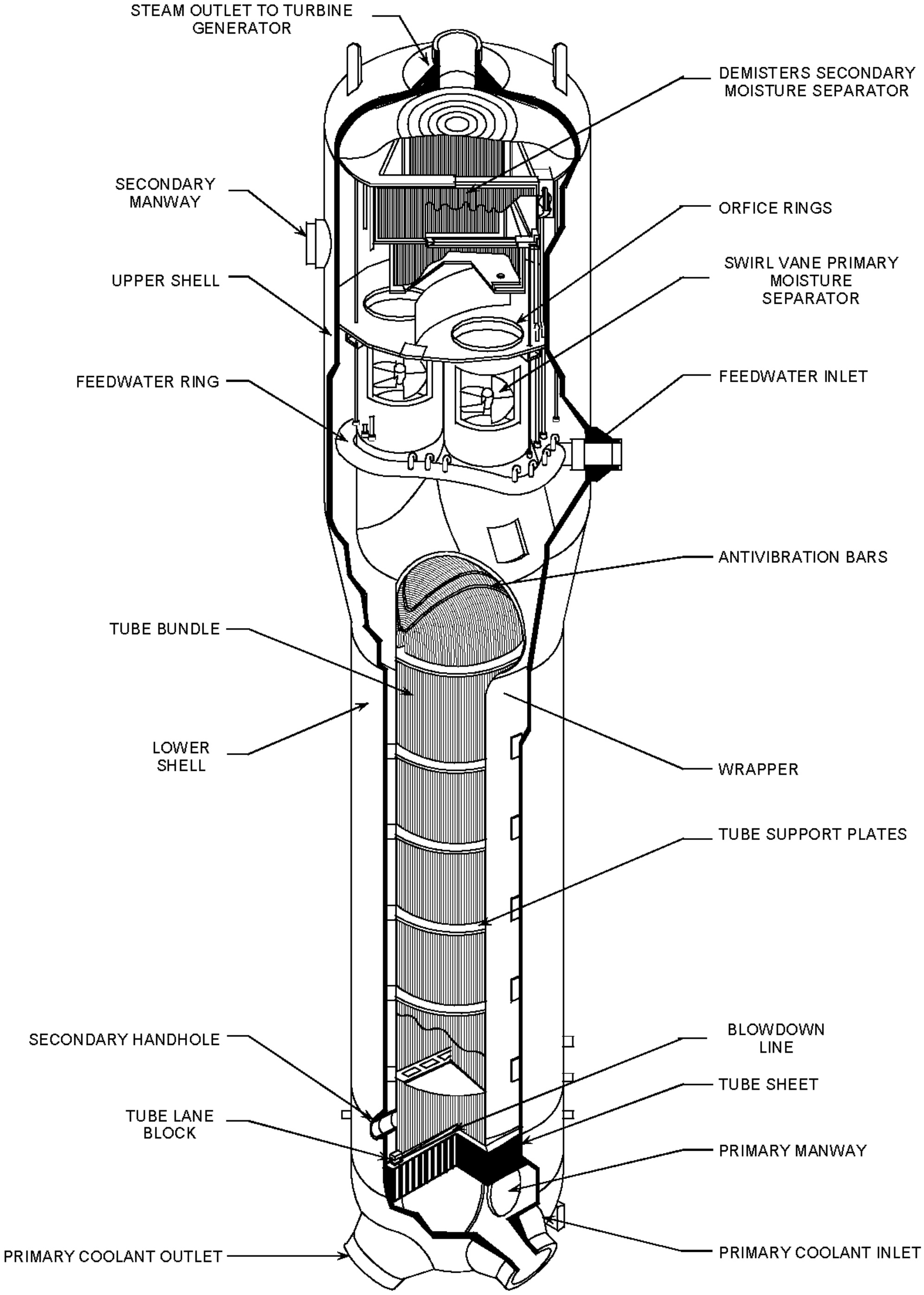

Figure 1.5: A Westinghouse Steam Generator [29].

1.4 Ringhals 4 unit

Ringhals 4 unit is a 3-loop Westinghouse design pressurized water reactor (PWR). Ringhals 4 was commissioned in 1982 with 2783 MW_{th} nominal power level. In 2011 the original Westinghouse PRZ and SGs were replaced with AREVA-design components and the turbines were modernized. As a result the reactor would have the potential to operate for 3300 MW_{th}. In the same year, the first start-up tests were performed with the new components in place, yet, the reactor was still licenced to operate at 2783 MW_{th} nominal power level. After three years of test operation new test were performed in March 2015 and the reactor was licensed to operate at 3300 MW_{th} nominal power level. The Load Step Test was among the tests performed in 2011 and 2015.

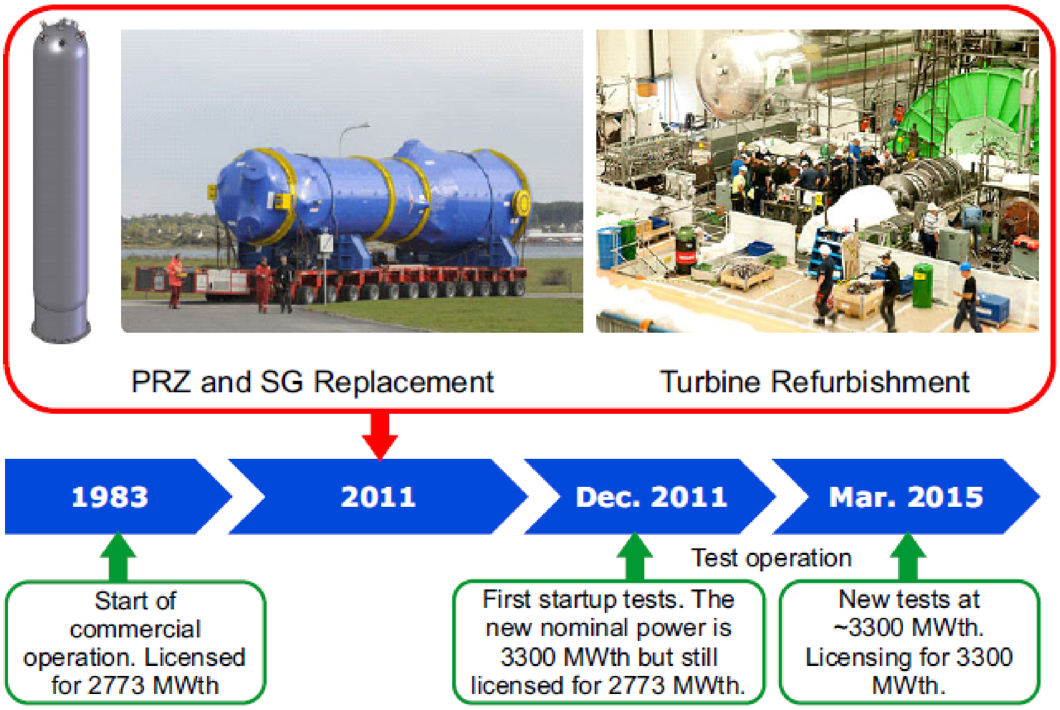

Figure 1.6: Timeline of Ringhals 4 unit [4].

1.4.1 The new SG

The new SG is more efficient than the old one due to its innovative design. The new features of the SG are the divider plate and the double wrapper which covers half of the bundle wrapper perimeter (figure 1.7). It is known from thermodynamics that the heat transfer in the SG depend on the temperature difference between the hot and the cold leg. Increasing the temperature difference translates to an increase in extracted heat from the fluid.

Hence, the droplets coming from the steam separator recirculates in the outer downcomer. 90 % in the hot side where the droplets are mixed in the bottom of the SG with the fluid in the hot leg, and 10 % in the cold side. As a result, the fluid temperature in the hot side increases.

At the same time feedwater is injected in the downcomer surrounding half of the bundle wrapper perimeter. The feedwater is mixed with the 10% of the recirculated droplets in the bottom of the cold side of the SG, and then both are mixed with the fluid flowing in the cold leg. Thus, the temperature of fluid in the cold side drops.

The divider plate separates the cold from the hot side of the SG so that this temperature difference is sustained. Consequently, more heat is extracted.

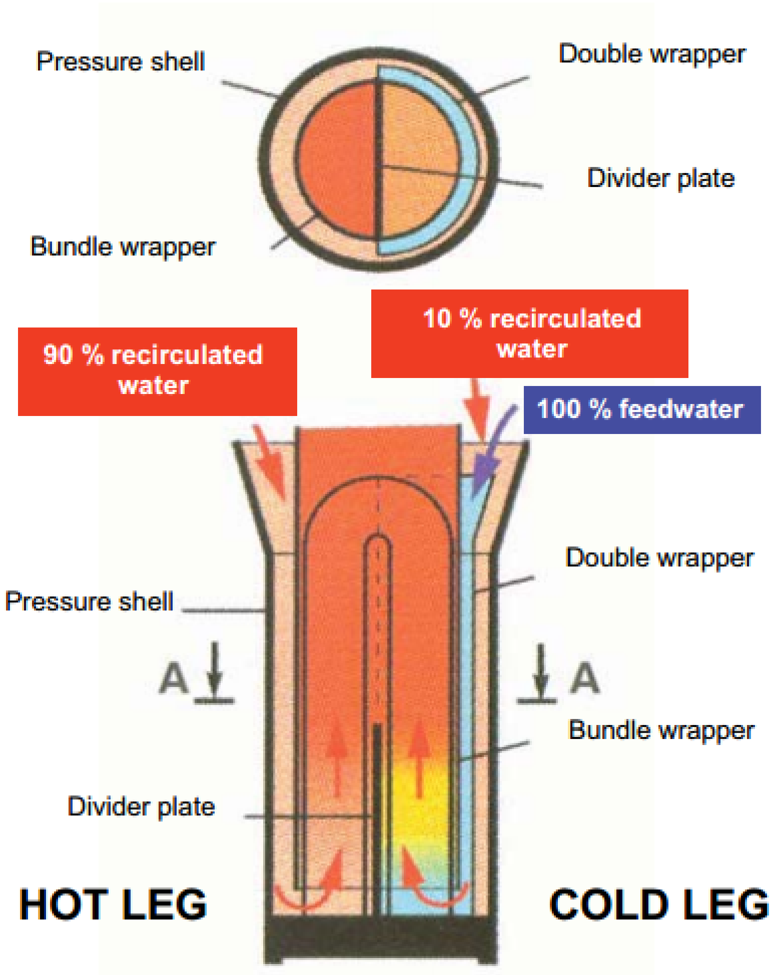

Figure 1.7: New SG of Ringhals 4 [5].

1.5 Aim of the thesis project

In general the aim of the present thesis project is the evaluation and assessment of the RELAP5 model of Ringhals 4 unit being used. More specifically, the calculated results are compared to measured plant data. The goal is to modify/improve the model and increase its predicting capabilities for reproduction of the calculated data as accurately as possible.

The ultimate goal is to obtain a RELAP5 model that will be capable of predicting every possible transient.

A new contribution of this master thesis is the assessment of the updated model using the FFTBM with signal mirroring. It is the first time in Sweden that this method is applied for the code assessment of a real plant start-up and maneuverability test.

1.6 Thesis outline

This thesis is divided in six chapters. Chapter 1 is a brief introduction in nuclear energy. It describes the principles of nuclear power production, the Pressurized Water Reactor (PWR) and the time-line of nuclear industry in Sweden.

Chapter 2 refers to RELAP5 model of Ringhals 4 unit. The most important parameters and features of the model are described, whereas chapter 3 is devoted to the Load Step performed at 2015-03-03. The reasons for the performance of this kind of experiment are mentioned and the experimental results are presented.

In order to run the whole transient it is essential for the code to achieve a calculated steady-state close to the real one, as indicated by the plant data. Hence, Chapter 4 is devoted to steady-state. The method used for achieving steady-state is explained and the calculated steady-state results are presented.

Chapter 5 deals with the analysis of the whole transient and the corresponding results are presented. Issues raised during the transient runs are described as well as the way they were mitigated. In the end of the chapter the most important outcomes of the transient analysis are summarized.

Chapter 6 is dedicated to Fast Fourier Transform Based Method (FFTBM) with signal mirroring. The outline of FFTBM is described as well as the results and the conclusions of code assessment quantification.For the FFTBM analysis, JSI FFTBM Add-in 2007 was used, an Excel 2007 application implemented by Dr. Andrej Prošek from Jožef Stefan Institute in Ljubljana.

Finally, chapter 7 presents an outline of the outcomes of this thesis, and elaborates on topics raised during steady-state and transient runs. Proposals for future projects are also included.

2
Modelling of Ringhals 4 Unit

The purpose of this chapter is to give some general information about the RELAP5 model of Ringhals 4. For the scope of this thesis RELAP5/MOD3.3 is used, which is the newest version of RELAP5 for the time being.

RELAP5 is a best estimate code used for the simulation of transients and postulated accidents. It is a generic code which can also be used for the simulation of other than nuclear thermal systems. It also plays an important role in licencing, evaluation of mitigation strategies and operational guidelines [5, 7].

Version RELAP5/MOD3.3 is based on a non-homogeneous non-equilibrium model for the two phase system which is solved using a partial numerical scheme [11]. It simulates important first-order effects related with transients in a simple manner so that the computational cost remains sufficiently low.

RELAP5 model of Ringhals 4 is a "stand alone" thermohydraulic model comprising of two main parts, the primary and the secondary side. It is a representation of the prototype reactor and as such it is the compromise between geometrical fidelity, results accuracy, complexity and cpu time. Inevitably, a number of simplifications are adopted as will be described in the remainder of the chapter.

2.1 Modelling of Primary Side

The most important major components included in the nodalization of the primary side in figure 2.3 are:

- The reactor pressure vessel (RPV).
- The pressurizer (PRZ).
- The safety and relief valves.
- The normal letdown.
- The main circulation pumps (MCPs).
- The residual heat removal system (RHRS).
- The charging system.

A description of the modelling of the most related major components follows in the upcoming subsections.

2.1.1 Modelling of Reactor Pressure Vessel

The core in the reactor pressure vessel (RPV) contains 157 fuel assemblies, each one modeled individually, and each one discretized axially into eight levels. Radially, the core is divided into three loops (figure 2.1) so that the code captures any possible asymmetric loop behaviour.

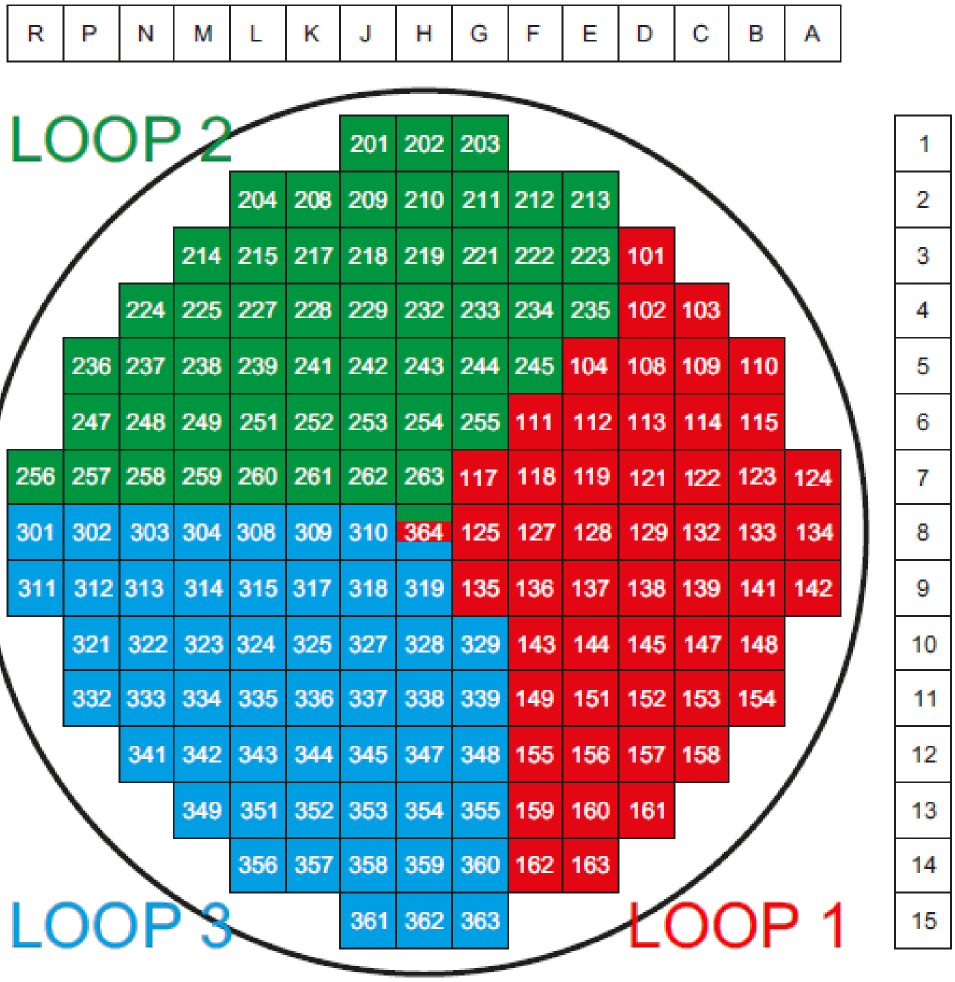

Figure 2.1: Radial discretization of the core of Ringhals 4 unit with 157 fuel assemblies[5, 7].

Another important feature in the modelling of the primary side is the connection of each loop is with three by-pass channels in order to simulate:

- The flow in space between the baffle and the barrel.
- The flow in the open guide thimbles.
- The flow in the core periphery.

Finally, the core inlet and outlet is represented by a bunch of interconnected junctions which are ultimately connected with the 157 fuel assemblies. This approach is chosen due to the RELAP5/MOD3.3 limitation that a "branch" component can be connected (with junctions) to maximum 9 other volumes.

2.1.2 Heat Source

So far, RELAP5 model of Ringhals 4 unit is not coupled with a neutronic code. As a result this model accounts only for the thermohydraulic features of Ringhals 4 unit, since the reactivity feedbacks and small variations in power cannot be accounted for. Thus, the thermal power is given as function of time (in a table form). Thermal power strongly affects a number of variables such as the primary pressure, fluid temperatures etc.

2.1.3 Modelling of PRZ

The PRZ is modelled as a pipe with 12 components (figure 2.2). The first two volumes in the bottom of the PRZ contain the proportional heaters and the ON-OFF heaters.

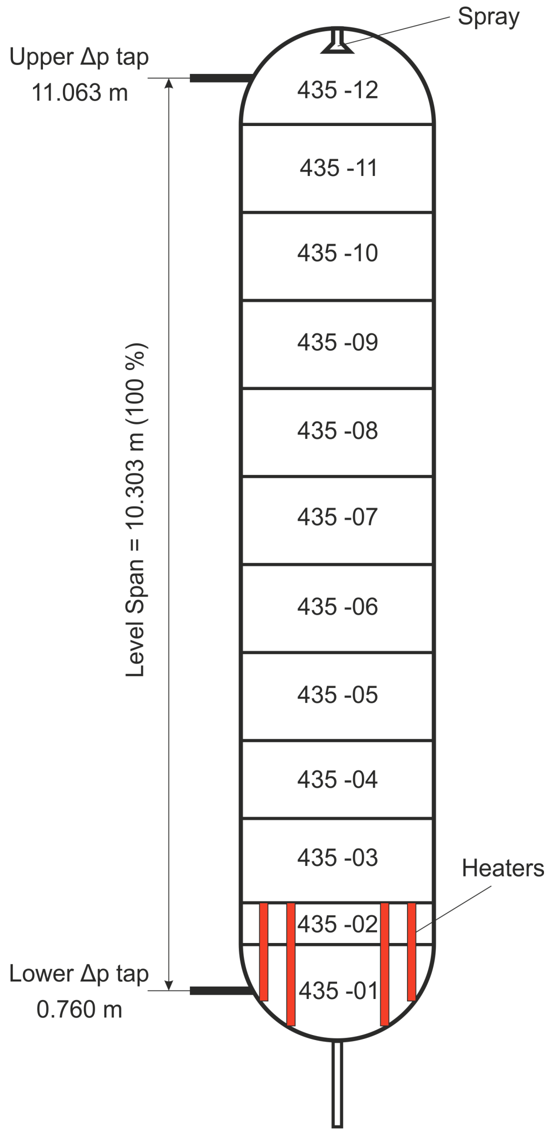

Figure 2.2: Nodalization of the PRZ [5].

Proportional heaters regulate moderate pressure deviations and their output is proportional to the pressure deviation from the nominal value, as their name indicates. Their maximum output is 375 kW. ON-OFF heaters operate at 1125 kW power output and they are actuated in case of larger pressure deviations.

The top volume of the PRZ is connected with the modelled spray nozzle (modelled as valve component) and the modelled power operated relief valve (PORV). In the real plant two spraying valves exist, each injecting maximum 14.52 kg/s, which are connected to cold legs of loop-1 and 2. In the current R4 RELAP5 model these two spraying valves are modelled as one, which is connected to the cold leg of loop-2, having 28.040 kg/s maximum flow rate.

2.2 Modelling of Secondary Side

As far as the secondary side concerned, the nodalization scheme presented in figure 2.5 includes the following major parts:

- The three hot legs (HLs) and cold legs (CLs).
- The three steam generators (SGs).
- The feedwater system.
- The steam dumping lines.
- The turbines.

As it is mentioned above, a number of simplifications take place in the model. For instance, the turbine and the condensers in the secondary side are not modelled. In such cases it is quite regular to use boundary conditions.

2.2.1 Modelling of Steam Generators

The nodalization scheme of a SG is presented in figure 2.6. Particularly, this is the nodalizaton scheme of SG-1, but the other two steam generators have exactly the same nodalization. The only difference lies in the first digit in the numbers assigned to each volume component. For instance, the inlet plenum in SG-1 is denoted as *control volume* 120 whereas in SG-2 as *control volume* 220.

2.2.1.1 Nodalization of SGs Primary Side

Water enters in the inlet plenum, volume 120, which is modelled as branch component, it flows along the U-tubes and exits from the outlet plenum, volume 140, which is modelled as branch component as well. U-tubes, volumes 130-01 to 130-22, are modelled as a pipe with 22 components. Water flows upwards in volumes 130-01 to 130-10, and downwards in volumes 130-13 to 130-22.

2.2.1.2 Nodalization of SGs Secondary Side

The description of the nodes below will follow the order of which they first appear to the incoming feedwater flow.

The inner downcomer of the SG receives feedwater from single junction component 868 and flows downwards through volumes 505-01 to 505-12. Then through single junction 508, water flows upwards starting from volume 510-01 which is the beginning of the cold side of the riser (vol. 510-01 to 510-07). Following the riser, water starts to boil in the boiler section, which is modelled by volume 530 (4 cells).

Volumes 535 (single cell) and 538 (3 cells) model the evaporator region where wet steam exists. This mixture flows upwards to the phase seperator, volume 540. Steam continues through the modelled steam dryers whereas the liquid droplets are driven to the upper part of the downcomer, volume 545-05, and then flow downwards to the outer downcomer, volume 550-01 to 550-13. Single junction 518 drives the water droplets in the hot side of the riser, volumes 520-01 to 520-07, where they flow upwards again.

It is important to mention that feedwater flowing to the inner downcomer 505 is being driven by single function 518 to the bottom of the cold part of the riser, volume 510-01, where mixing occurs with the droplets coming from the outer downcomer (vol.550-01 to 550-13).

The steam driers and the steam dome are modelled by volumes 560 and 570 respectively.

Volumes 510-01 to 510-07 of the cold side of the riser are thermally connected to volumes 130-16 to 130-22 of the modelled U-tubes. Volumes 520-01 to 520-07 are thermally connected to volumes 130-01 to 130-07 of the modelled U-tubes. Likelywise, volumes 550-01 to 550-13 are thermally connected to volumes 505-01 to 505-12 and to volumes 520-01 to 520-07 as well. In the same trend, volumes 520-01 to 520-07, volumes 510-01 to 510-07, volumes 130-01 to 130-07 and volumes 130-16 to 130-22, are thermally interconnected to each other.

It should also be mentioned that the upper part of the downcomer appears both in the left and in the right side of the nodalization scheme as if they were two distinct volumes. They constitute one volume though.

In addition, all the volumes of the SG model where flow occurs are modelled as pipe components.

2.2.2 Turbine Modelling

It is a common practise to model the turbines as boundary conditions (vol. 814 and 824). A thorough modelling of the turbine has been proven to be very complicated. Thus, the turbine is replaced with a time dependent volume, in which temperature/quality and pressure have to be defined accordingly so that the model reproduces (as much as possible) the test data.

2.2.3 Inflow Boundary Condition

The inflow boundary condition refers to the conditions in time dependent volume 851. The pressure and temperature are set as function of time.

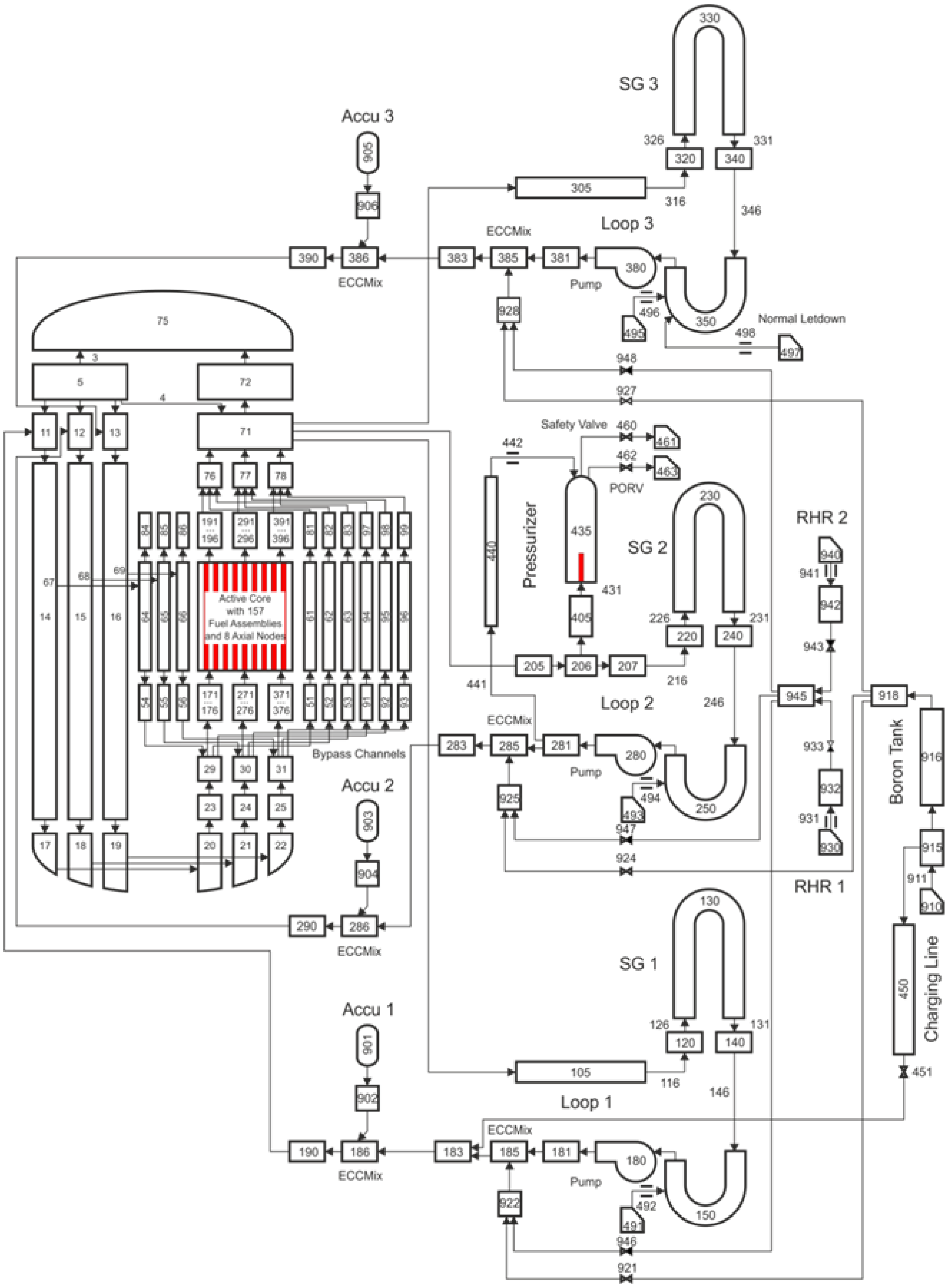

Figure 2.3: Nodalization scheme of the primary side of Ringhals 4 unit [5, 7].

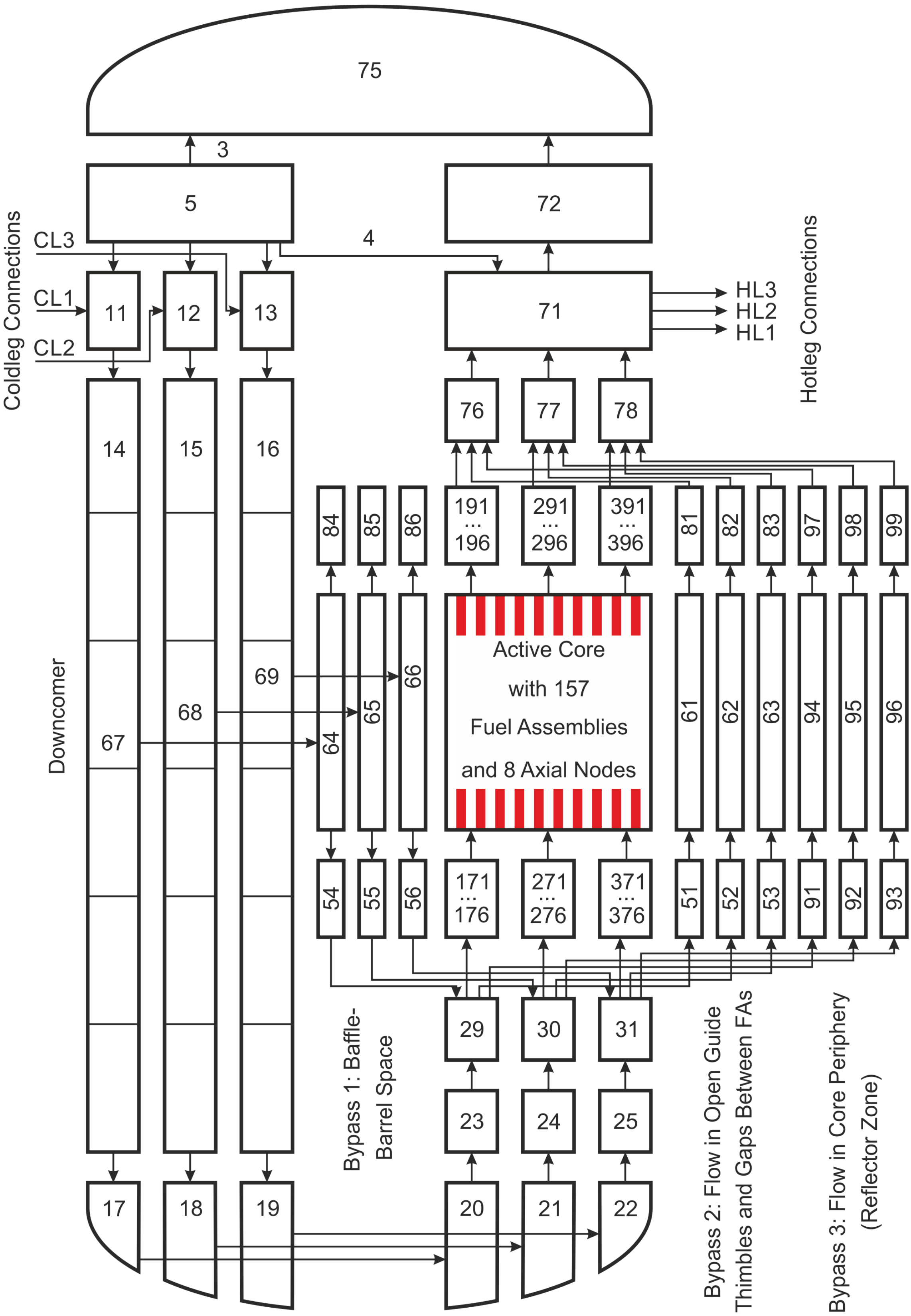

Figure 2.4: Nodalization of the core. [5, 7].

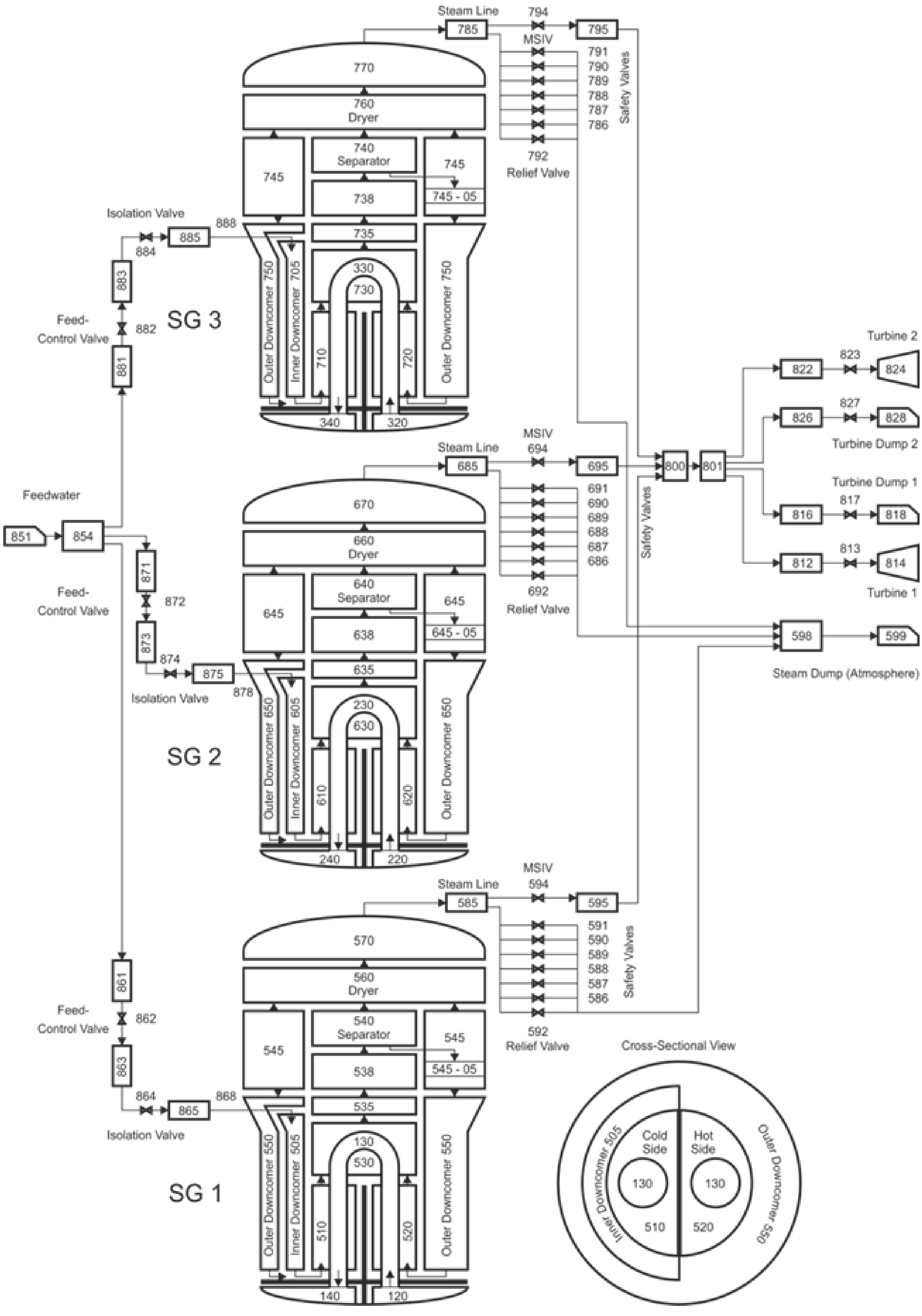

Figure 2.5: Secondary side discretization of Ringhals 4 unit [5, 7].

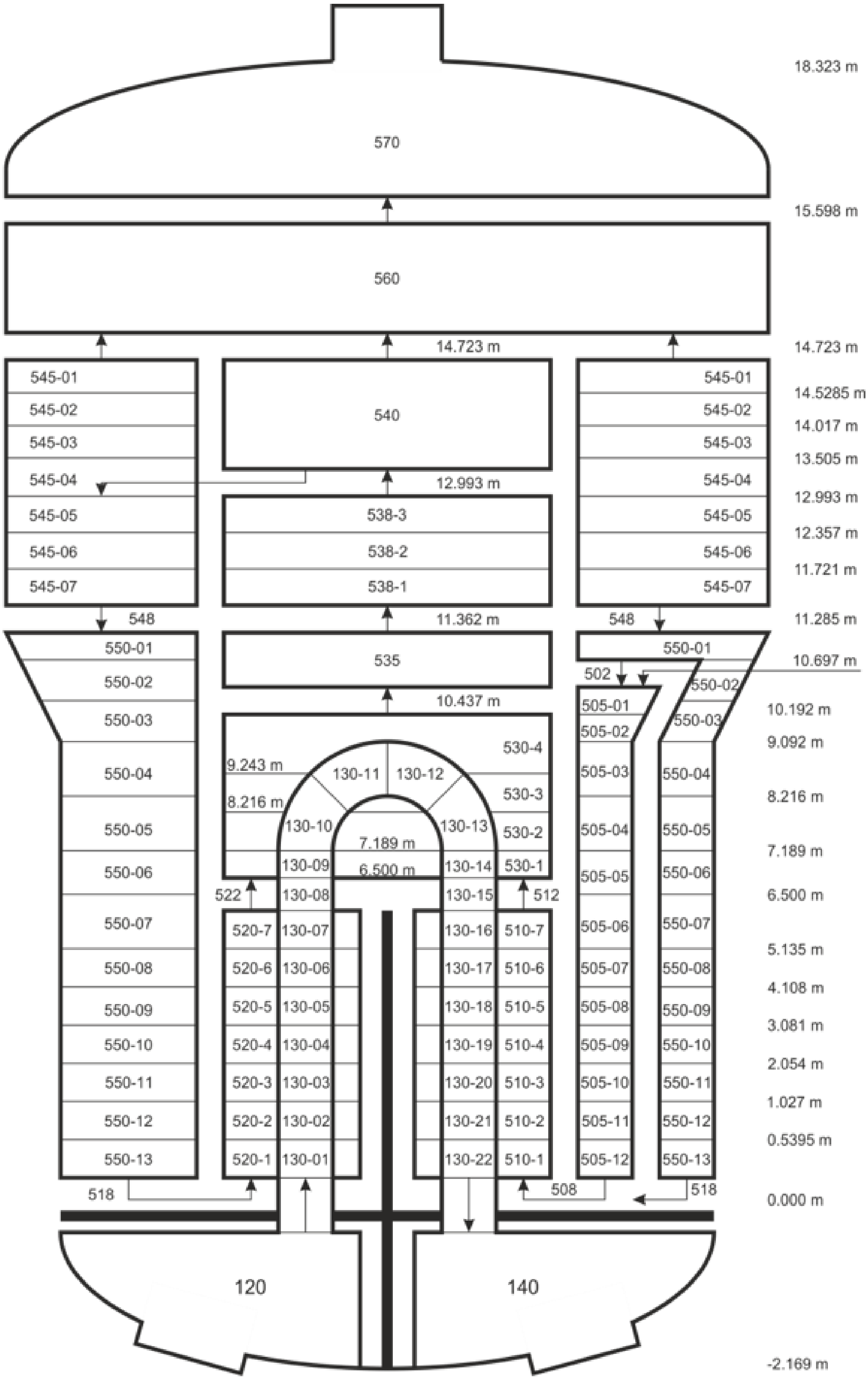

Figure 2.6: Nodalization of the SG. [5, 7].

3

The Load Step Test

The purpose of the Load Step Test is to verify that the control systems are capable to handle the rapid power perturbation without the need of activation of any safety systems.

The Load Step Test can essentially be divided in five phases which are evident by observation of figure 3.1:

- ***Phase 1 - Initial Steady-State***: This stage corresponds to the initial state of the plant just before the rapid power decrease.
- ***Phase 2 - Power Decrease***: The turbine power is sharply reduced by 10 %. Control rods are rapidly inserted in the core so that the thermal power level reduces approximately 10 %.
- ***Phase 3 - Intermediate Steady-State***: Turbine power is kept constant at the -10 % reduced power level. Primarily with control rod maneuvering the reactor is stabilised to the new thermal power level, approximately 10 % lower than the initial one.
- ***Phase 4 - Power Increase***: Turbine power sharply increases by 10 % and is restored to the its initial value. Control rods are rapidly withdrawn in order to increase the thermal power level by 10% reaching the thermal power level of *phase-1*. Nonetheless, the thermal power level overshoots and it peaks at a power level greater than that of the initial steady-state of *phase-1*, but gradually decreases to the level of the initial steady-state.
- ***Phase 5 - Stabilizing to the Initial Steady-State***: Turbine power is kept constant to its initial/nominal power level. The reactor is gradually stabilized to the initial steady-state.

The results of the Load Step Test are presented in the graphs below. For the test measurements usually three channels are used for each variable. Some variables, such as the pressure in the SGs or in the steam lines, have to be measured for each of the SGs and steam line respectively. Three channels are used for each component. Some other variables are measured using two channels, such as the PRZ controllers output signals in figure 3.11, and few with only one channel.

As it can be seen from the figures the measurements slightly differ for every component. Yet, they follow the same trend. The oscillating nature of the measurements is also obvious. For each component variable the measurements of the different channels are averaged in order for the data to be processed. In the same trend, similar variables for multiple components are averaged.

However, for the level in the PRZ the channel with the lowest level measurements is chosen. This is in conformity with the configuration in the prototype reactor. The operator chooses which of the three channels will be used for the real-time monitoring of the level in the PRZ.

It is worthy to mention that there is not any direct test data regarding thermal power, neither the thermal power level that the reactor operates at is a priori known. The thermal power must implicitly be estimated using other test data. One indicator about how the thermal power evolves over time is the neutron flux, which is however not linearly related with the thermal power level due to reactivity feedbacks.

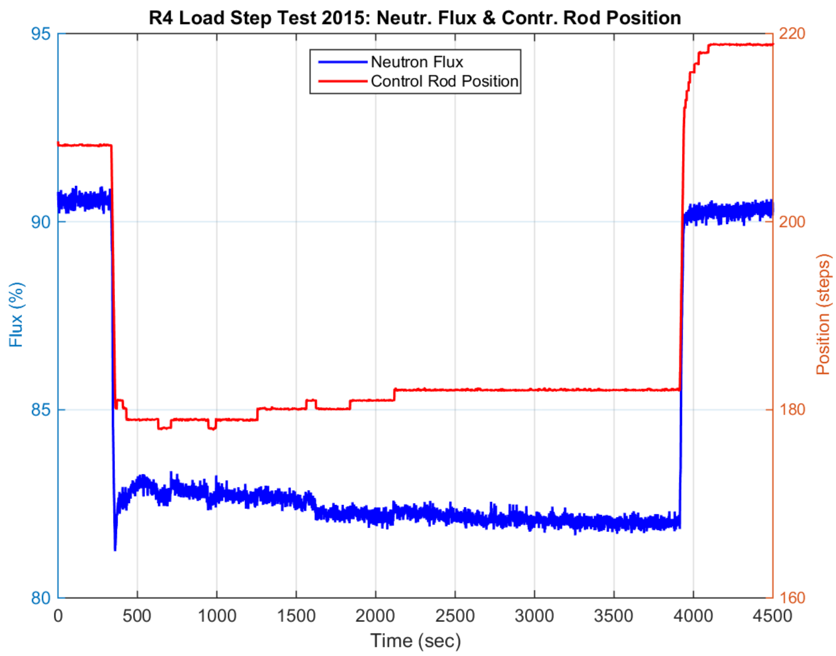

Figure 3.1: Neutron flux and control rod position.

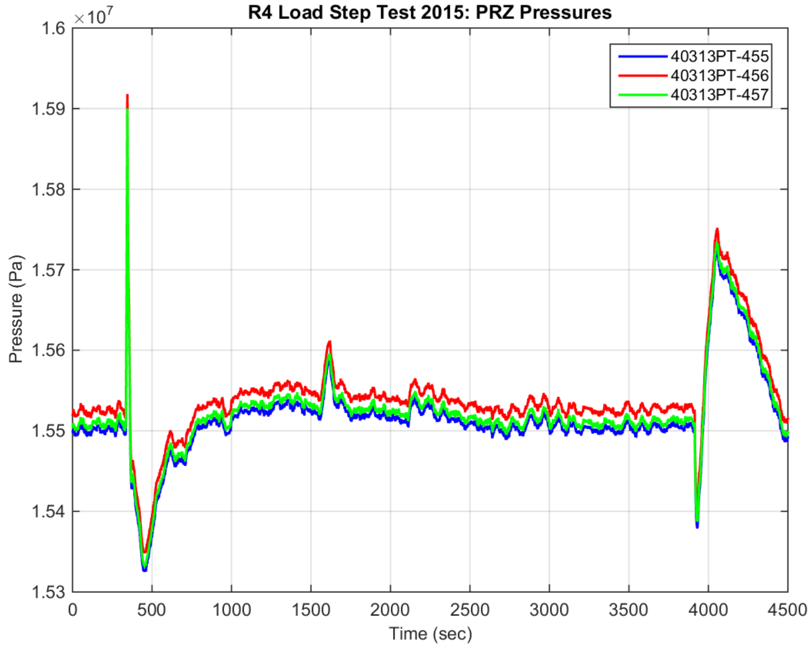

Figure 3.2: Pressure in the PRZ with time measured by three different channels.

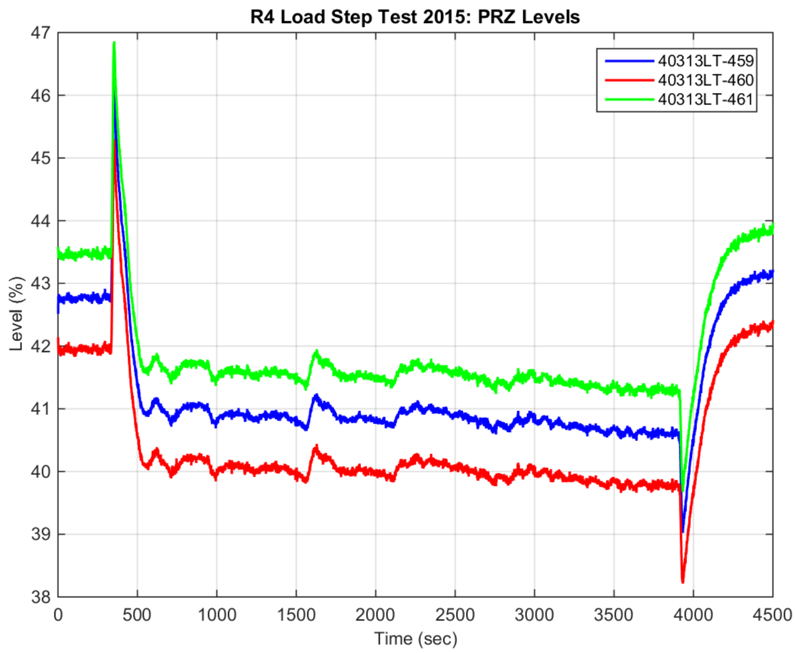

Figure 3.3: Level in the PRZ measured by three different channels.

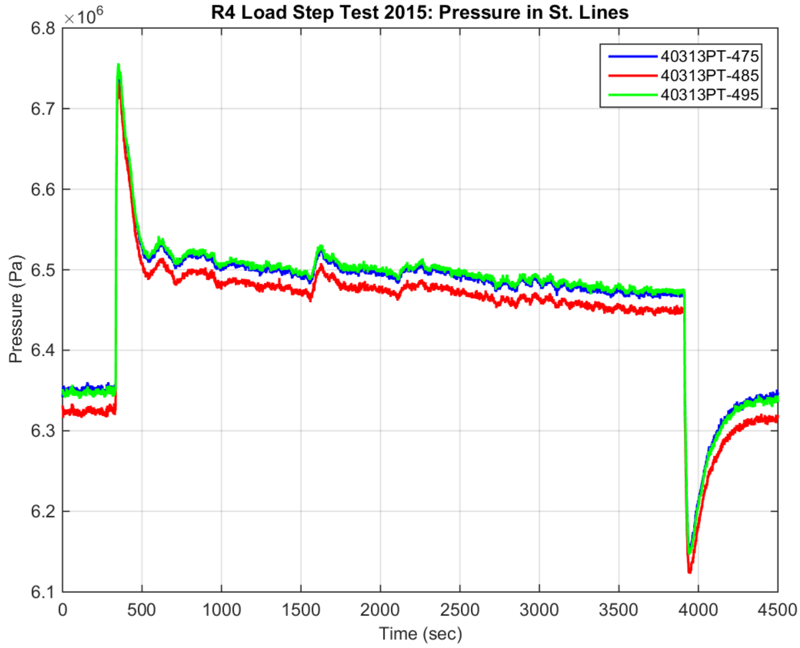

Figure 3.4: Pressure in the steam lines as measured by the first channel of each steam line.

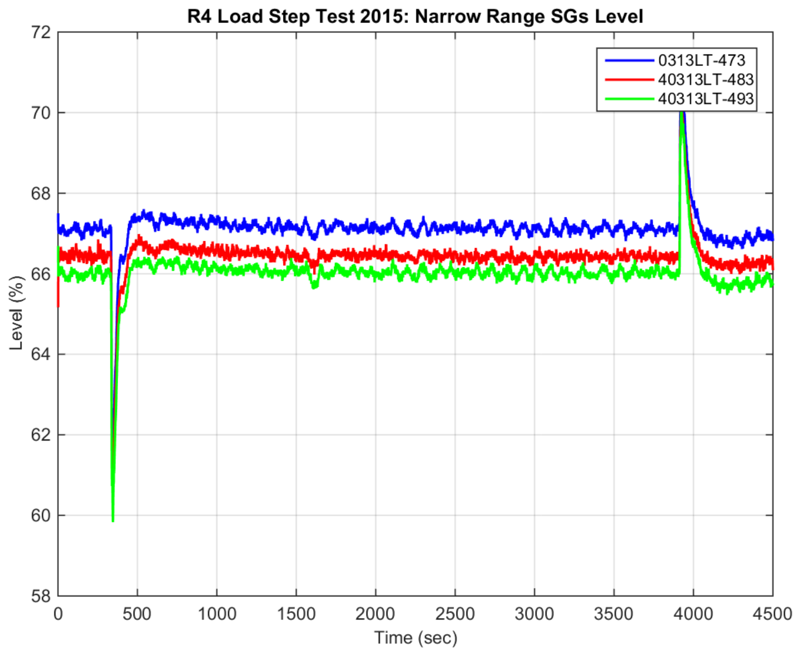

Figure 3.5: Level in SGs as measured by the first channel of each SG.

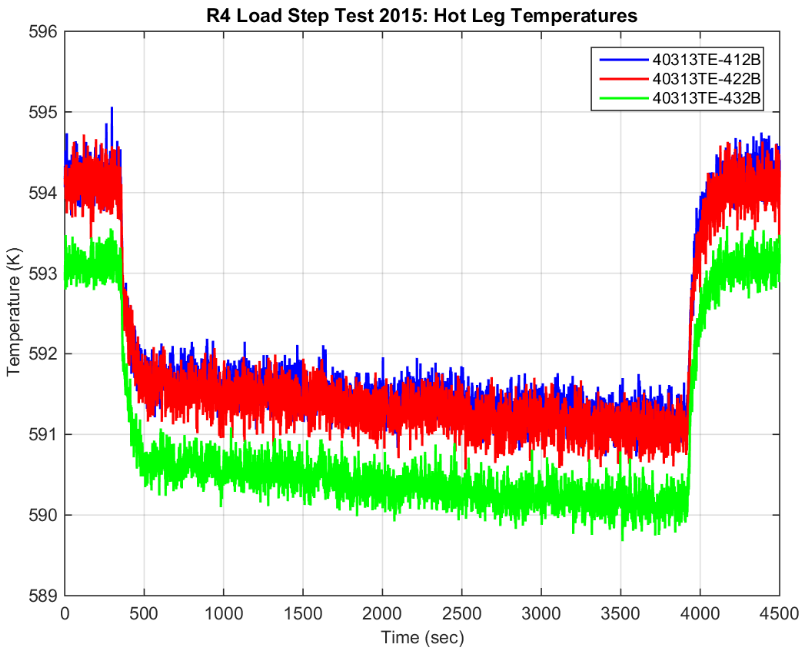

Figure 3.6: Temperature in the hot legs as measured by the first channel of each hot leg.

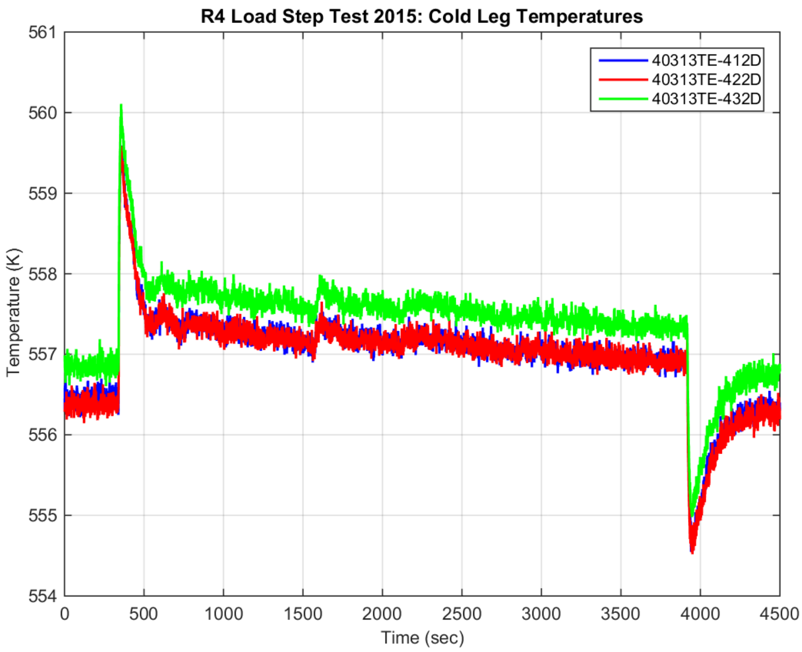

Figure 3.7: Temperature in the cold legs as measured by the first channel of each cold leg.

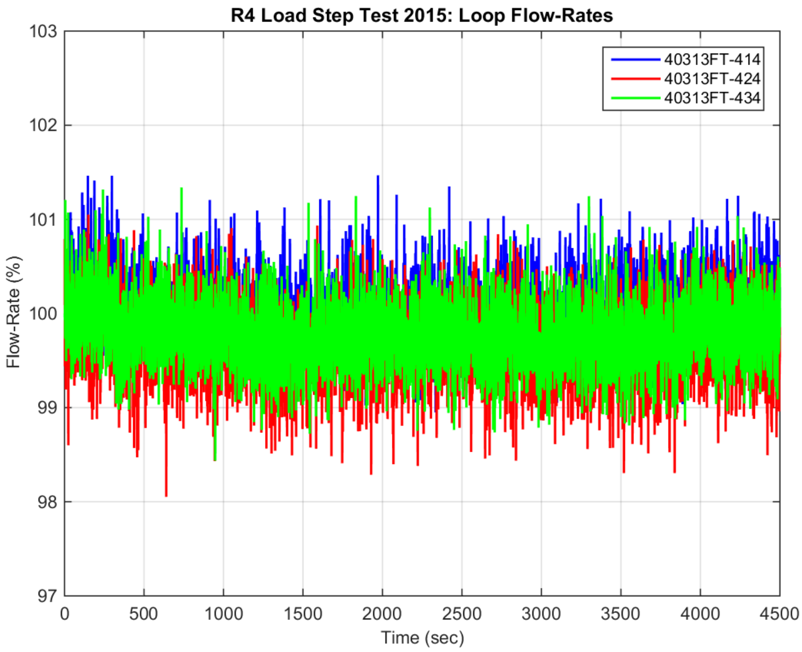

Figure 3.8: Flow-rate in the three loops as measured by the first channel of each loop.

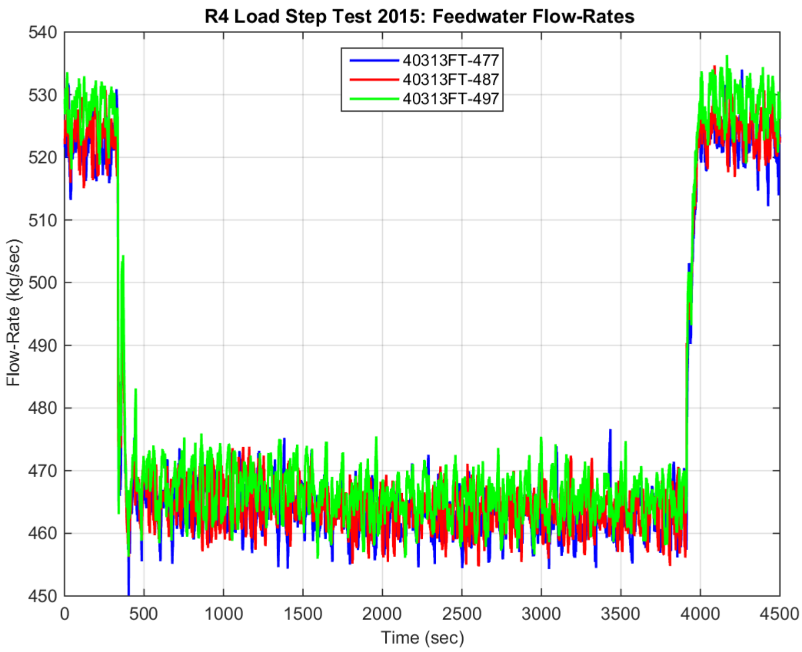

Figure 3.9: Feedwater-flow rate in the three loops measured by three different channels.

Figure 3.10: Steam-flow rate in the three steam lines as measured by the first channel of each steam line.

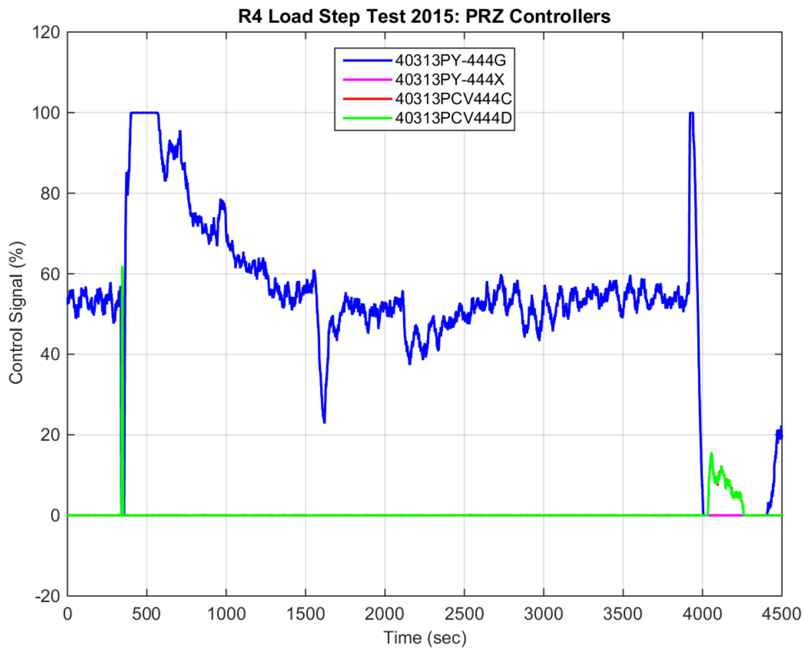

Figure 3.11: Spraying flow controllers output signals (red and green lines) and proportional heaters controller output signals (blue and magenta lines), each measured by two channels.

4

Load Step Test Analysis (1) - Calculating Steady-State

The first phase of the Load Step Test is a steady-state. Therefore the model should realistically simulate the initial steady-state before the simulation of the other phases of the transient.

So, the first section of this chapter deals with achieving steady-state using the previous model of Ringhals 4 tweaking (slightly) specific parameters. The second section elaborates on strategies to reach steady-state whereas the third presents the calculated results.

4.1 Achieving Steady-State

The code has to be fed with an appropriate input deck. In other words, the variables needed for the code to run must be initialized (e.g. the normalized thermal power level). It has to be stated that the initial guess for the initial values of the input deck have to be realistic enough. The control systems simulated in RELAP5 of R4 eventually force all variables to reach a steady-state value. But in case of an unrealistic input deck the initial values the control systems greatly overshoots trying to stabilize the system and more computational time and resources are needed.

It is also important that all the variables have finally set to a constant value during the steady-state runs time interval. In case they do not, it means that the modelled reactor is still in transient mode and the results of the following the transient runs will be distorted.

So, how one could make a good guess for the initial values of the input deck? The answer is by exploiting the initial steady-state test data (measured data corresponding to the first phase of the load step test). But a quick overview of the test data reveals that some of the required input parameters have not been measured, like the thermal power, whereas some others are not measured in SI units (e.g. the pressure in the PRZ is measured as overpressure). RELAP5 requires all the input parameters in SI units. For instance, the loop flow-rate (figure 3.8) is measured in [%] and unfortunately the value which is normalized is not known. The same happens with the neutron flux which is given in [%] but the normalizing value is not known.

As a result, the best strategy to initialize the required input variables that are missing is to assume the behaviour of the reactor symmetrical (e.g the conditions at every steam line and SG are the same) and perform a heat balance calculation using averaged values for the three SGs. Thus, using the plant data for the initial steady-state period, $0 - 338\ s$, the following quantities are calculated as averages of the corresponding values in the three SGs:

- Feedwater flow-rate.
- Steam flow-rate.
- Hot and cold leg temperature.
- Pressure in steam line.

The conditions (pressure and temperature) in the charging line of the secondary side are calculated too, using the plant data for $0 - 338\ s$. Hence, everything is ready to perform the heat balance calculation:

Secondary Side

$$\begin{aligned}
\dot{m}_{fw} &= 524.57 kg/s \\
T_{fw} &= 480.92 K \\
h_{fw} &= 0.889723 \times 10^6 kJ/kg \\
\dot{m}_{steam} &= 517.17 kg/s \\
P_{steam} &= 64.31 bar \\
x_{steam} &= 1 \\
h_{steam} &= 2.7797 \times 10^6 kJ/kg \\
\bar{\dot{m}} &= (\dot{m}_{FW} + \dot{m}_{steam})/2 = 521.37 kg/s \\
Q_{SG} &= \bar{\dot{m}}(h_{steam} - h_{fw}) = 985.38 MW \\
Q_{secondary} &= 3 \times Q_{SG} = 2956.13 MW
\end{aligned}$$

Primary Side

$$\begin{aligned}
Q_{primary} &= Q_{secondary} \\
P_{PRZ} &= 154.99 bar \\
T_{HL} &= 593.68 K \\
T_{CL} &= 556.51 K \\
h_{HL} &= 1.45632 \times 10^6 J/kg \\
h_{CL} &= 1.24997 \times 10^6 J/kg \\
\dot{m}_{loop} &= Q_{SG}/(h_{HL} - h_{CL}) = 4775.27 kg/s \\
\dot{m}_{total} &= \sum_{i=1}^{3} \dot{m}_{loop,i} = 3 \times \dot{m}_{loop} = 14325.81 kg/s
\end{aligned}$$

where $\dot{m}_{fw}$ and T_{fw} the mass flow-rate and the temperature of the feed-water, Q_{SG} the heat produced by one SG, $Q_{primary}$ the heat produced in the core and $Q_{secondary}$ the total heat in the secondary side produced by all SGs.

4.1.1 Strategies to reach Steady-State

The step following the input deck variables initialization is setting the set-point values in the controllers. The set-points are set accordingly using the components averaged values for the corresponding test data during the initial steady-state period $0 - 338\ s$.

Then, with the set-points set and the desirable values set the user should vary the turbine boundary conditions conditions (pressure),the thermal power level and slightly the pump speed, as long as results close to the expected/desired values are obtained (table 4.1). This procedure is time and cpu costly to be performed manually. Hence, a new control system has been embedded in the model, which varies the pressure of turbine boundary condition so that the SG pressure reaches the desired value. This auxiliary control system must be deleted in the transient runs.

As for the primary pressure the model offers the option to connect the top of the pressurizer with a time dependent volume (time dependent vol. 439 - it does not appear in the nodalization diagrams) which has pressure equal with the PRZ pressure set-point. This time dependent volume acts like a huge steam tank which when connected with a smaller volume, the PRZ , it forces the PRZ pressure to be equal. The connection between the PRZ and the time dependent volume should be eliminated when the transient runs start.

However, another method was applied. The PRZ pressure control system was let to run sufficiently long, in order to converge the pressure to the desired value.

4.2 Steady-State Results

Several steady-state runs were launched, each one with a duration of 6000 s, modifying mostly the thermal power and to less extent the pump speed.

A constant negative primary pressure deviation from the PRZ pressure set-point was observed in the last seconds of the transient runs. The modeled PRZ control systems configuration was investigated and it turned out that for this primary pressure deviation the proportional heaters didn't function close to their working point, almost 50 % capacity at 0 % primary pressure deviation, but around 38 % capacity. This means not only improper functioning of the proportional heaters at steady-state but less heating than expected for the stabilization of PRZ pressure in its steady-state value. Consequently, the heat balance of the PRZ was checked (heat structure 435) and it was found to be imbalanced. As a result, less heat was exerted from the PRZ walls than was inserted. In other words an excess amount of heat were remaining in the PRZ causing the overestimated pressure in the PRZ (improper capacity of proportional heaters).

From the efforts described above it was concluded that the formerly estimated 200 mm thickness of the PRZ insulation was unrealistic, and it was reduced to 10 mm. In the new series of steady-state runs with 10 mm insulator thickness, the working point of the proportional heaters is restored close to 50 % as the primary pressure almost coincides with PRZ pressure set-point.

Thus, with the new PRZ insulator thickness and after several initializations and runs the initial conditions of table 4.1 give the best steady-state values which are presented in the figures below.

The best steady-state values achieved are presented in the following table and to the figures below.

Parameter	Desired	Achieved	RELAP5 Parameter	set-point Setting
Thermal Power (MW)	2950	2950	cntrlvar-1	cntrlvar-1
PRZ Pressure (bar)	154.99	155.04	p-43512	cntrlvar-400
PRZ Level (%)	41.72	41.71	cntrlvar-430	cntrlvar-430
Hot Leg Temp. (K)	593.68	593.67	tempf-12001	automatic
Cold Leg Temp (K)	556.51	556.42	tempf-14001	automatic
Average Loop Temp (K)	575.10	575.13	cntrl-434	automatic
SG Pressure (Pa)	64.31	64.40	p-57001	p-81401,82401
SG Level (%)	66.71	66.71	cntrlvar-502	cntrlvar-503
SL Pressure (Pa)	6347000	6338119	p-58505	p-81401,82401
Loop Flow-Rate (kg/sec)	4775.27	4772.56	mflowj-18001	cntrlvar-180
Feedwater Flow-Rate (kg/sec)	521.37	519.32	mflowj-86800	automatic
Steam Flow-Rate (kg/sec)	521.37	519.39	mflowj-59400	automatic
Feedwater Temp. (K)	480.92	480.92	tempf-85100	tempf-85100

Table 4.1: Steady-state values achieved and expected/desired values according to the test data.

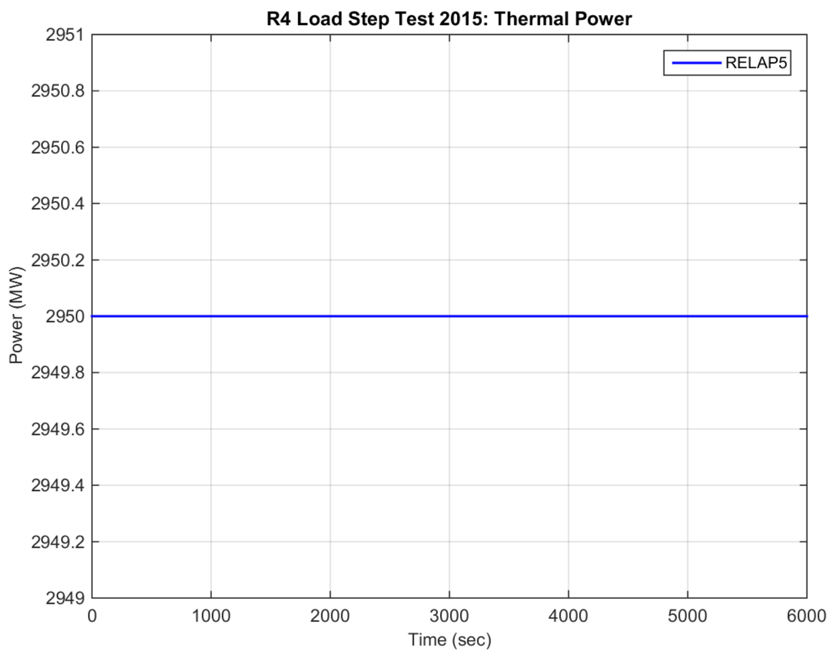

Figure 4.1: Thermal Power.

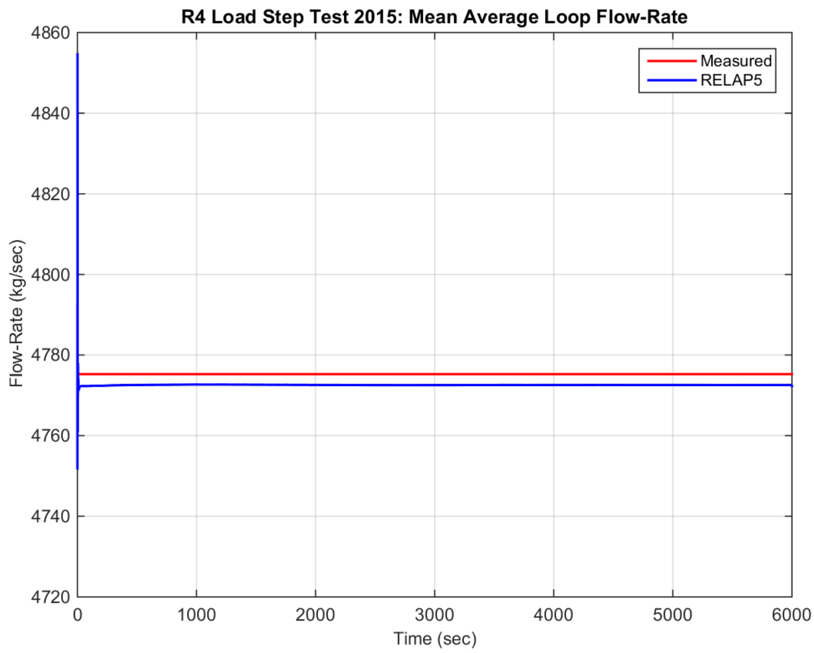

Figure 4.2: Loop flow-rate.

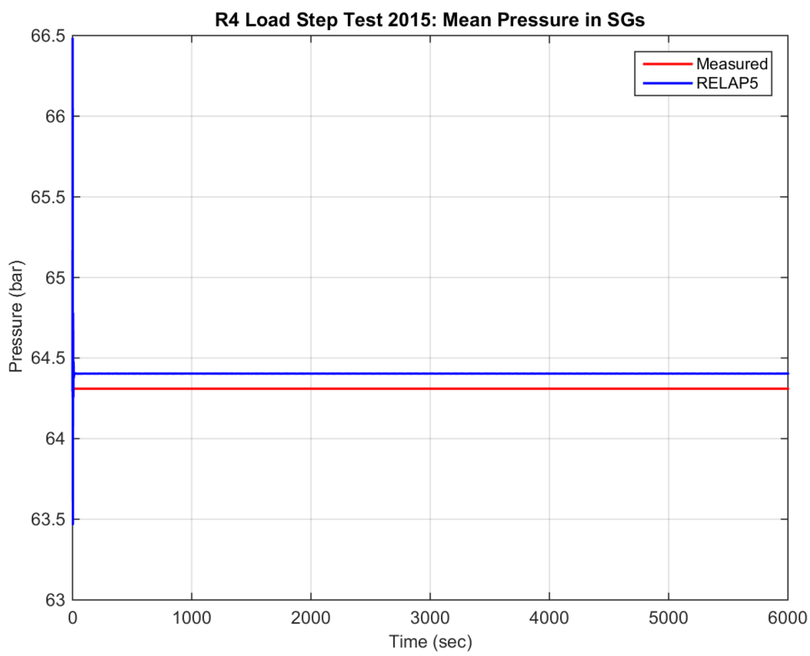

Figure 4.3: Pressure in SGs.

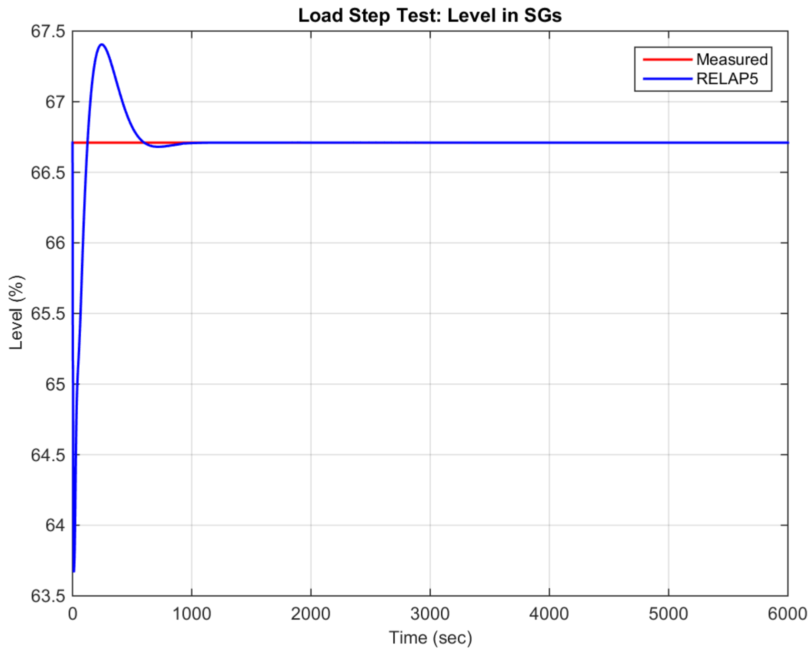

Figure 4.4: Level steady-state value in the SGs.

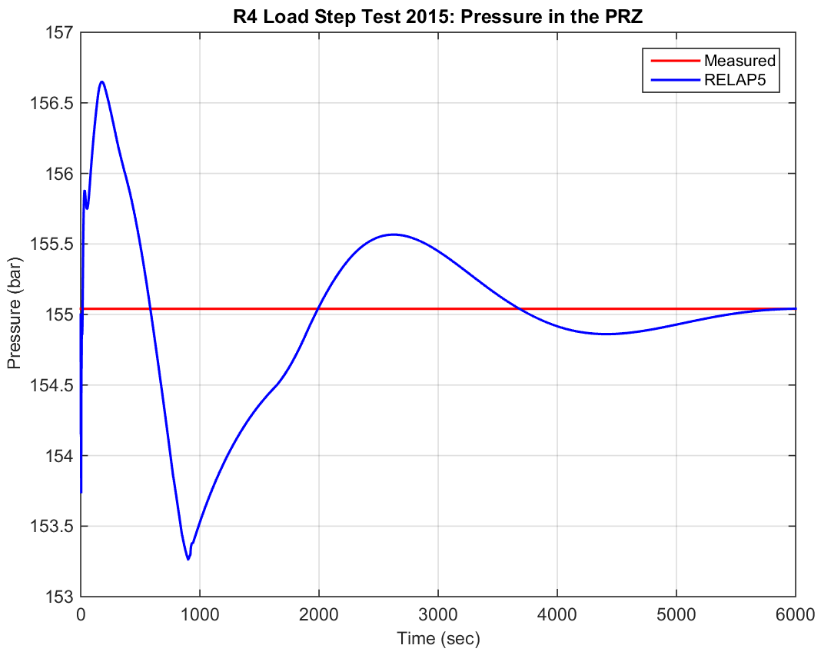

Figure 4.5: Pressure in the PRZ.

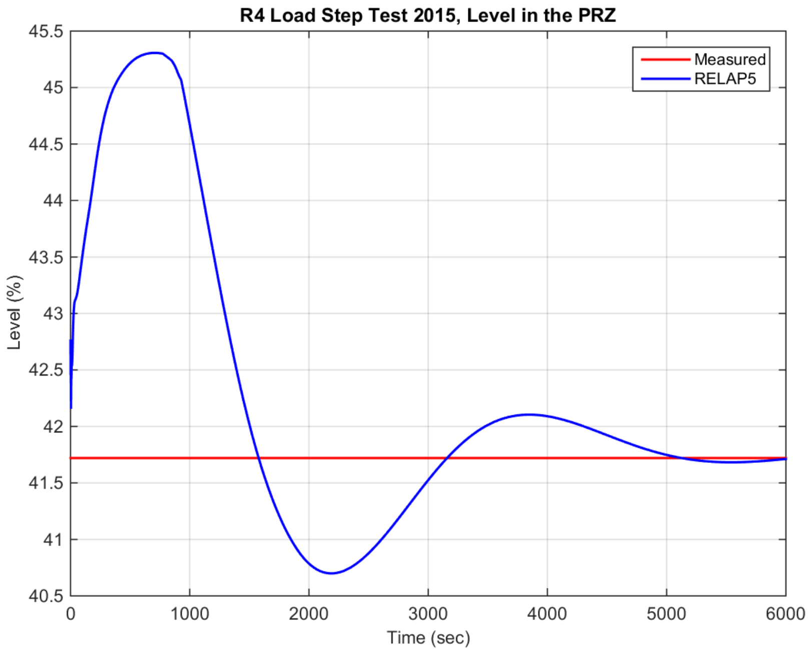

Figure 4.6: Level in the PRZ.

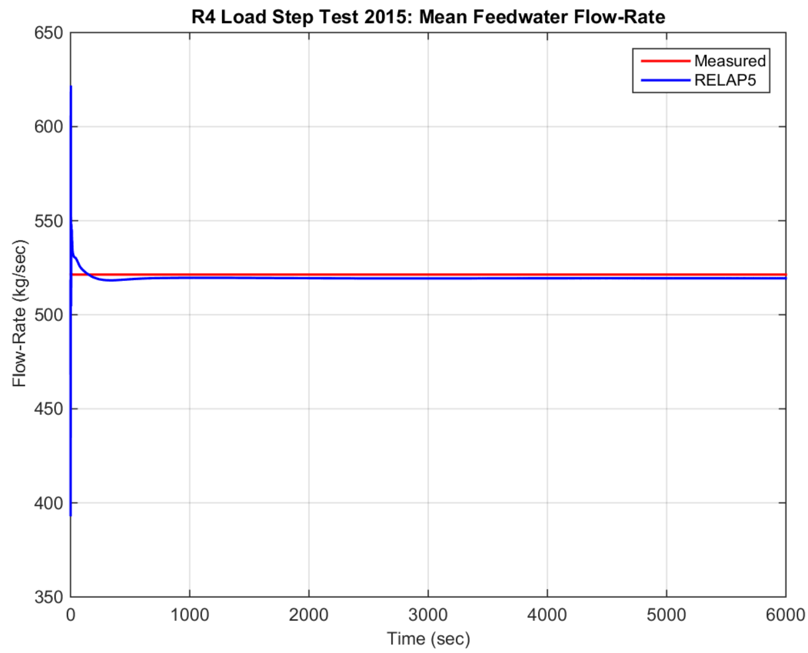

Figure 4.7: Feedwater flow-rate.

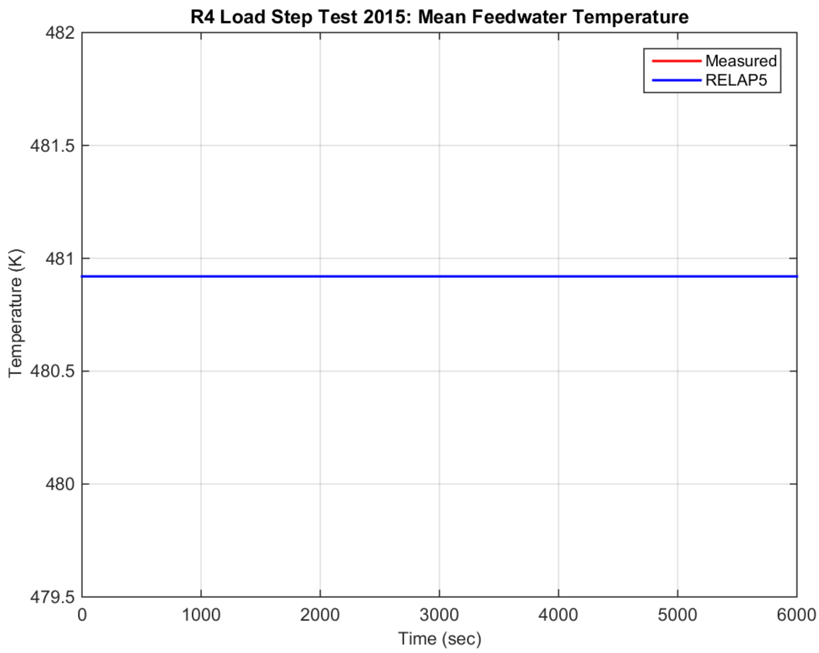

Figure 4.8: Feedwater temperature.

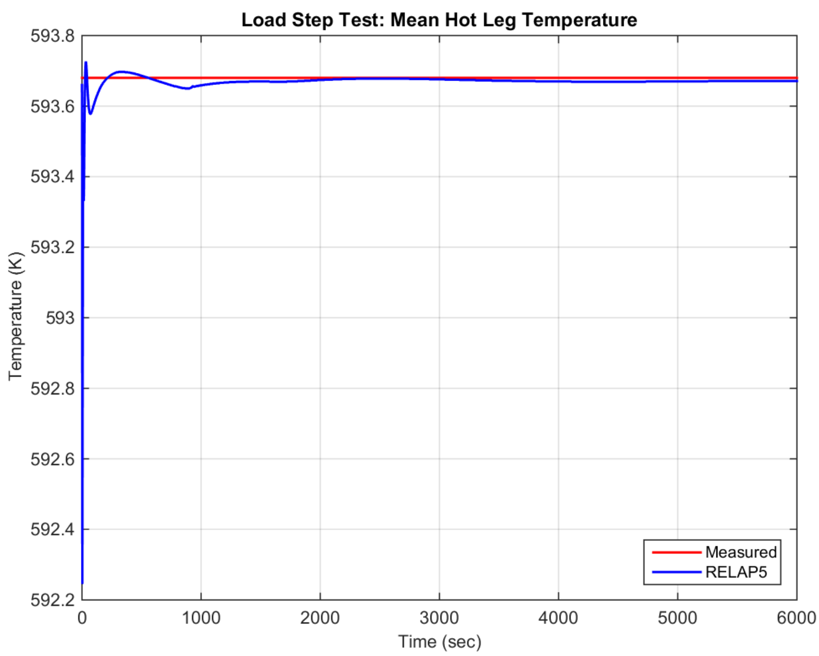

Figure 4.9: Temperature in hot leg.

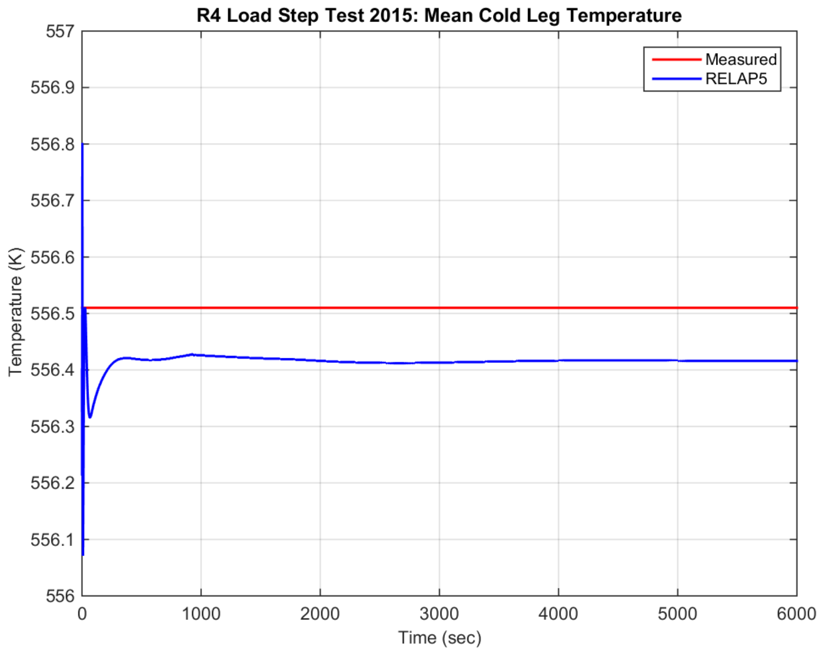

Figure 4.10: Temperature in cold leg.

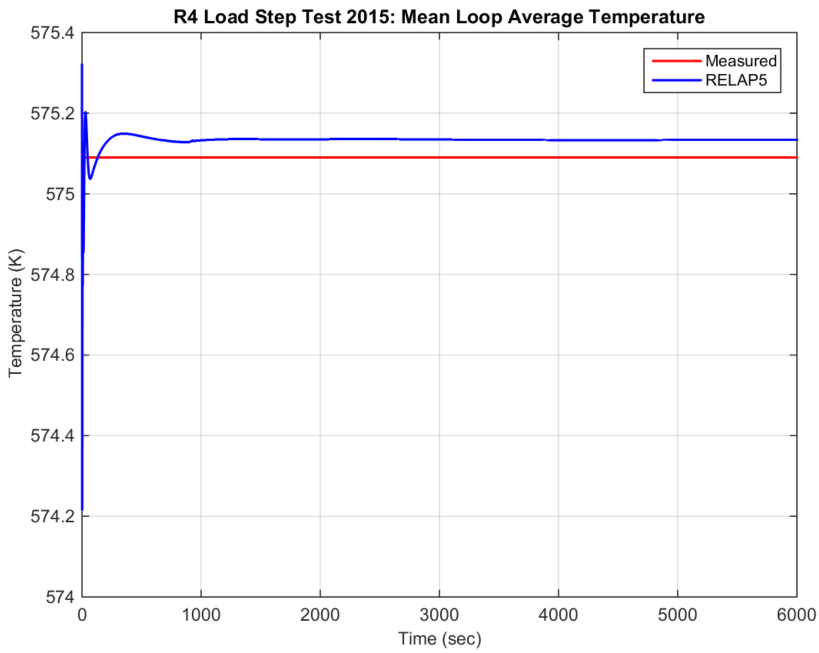

Figure 4.11: Average temperature for the three loops in the hot leg.

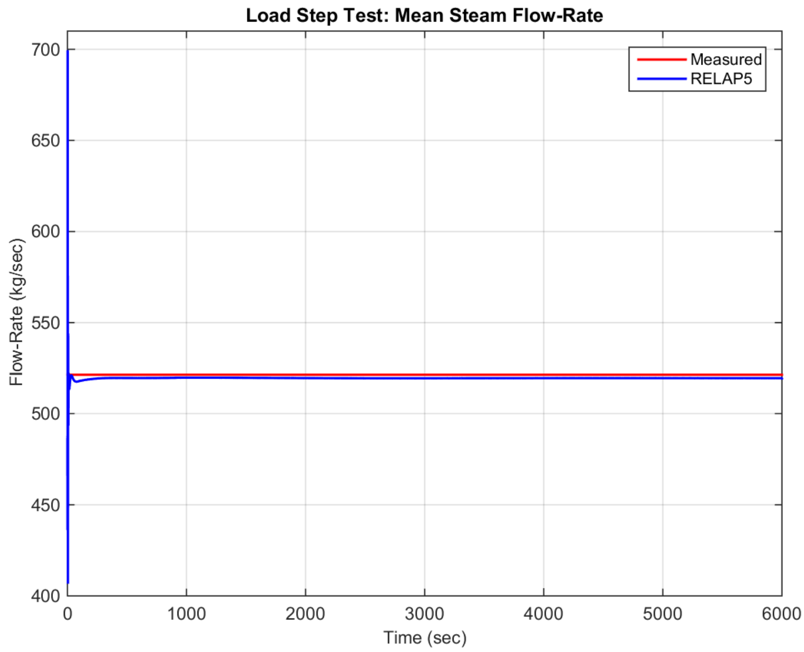

Figure 4.12: Steam temperature.

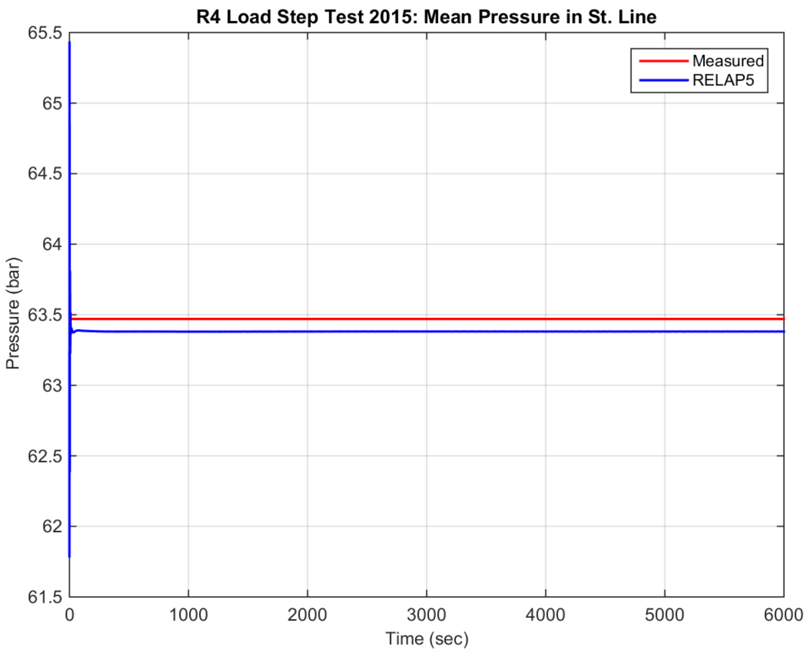

Figure 4.13: Steam pressure.

It can be concluded from table 4.1 and from the figures above that all the variables converge during the 6000 *s* duration of the steady-state runs. Some of them, like the pressure in the steam lines (figure 4.13) and the pressure in the SGs (figure 4.3), converge fast, whereas others, like the hot leg temperature (figure 4.9) and the pressure in the PRZ (figure 4.5) need thousands of seconds to converge. The goal of reaching a realistic steady-state by the code is fulfilled. The next step is the initiation of the transient runs, each of 4500 *sec* duration, starting from the end of the most successful steady-state run presented above.

5

Load Step Test Analysis (2) - Transient Analysis

Analysis of the whole transient takes place in this chapter. Transient runs begin at the end of the steady-state runs. After each run the calculated results are compared against the test data. Experience has shown that when the calculated secondary pressure matches with the corresponding measured values, the other variables tend to converge to their measured values as well. Hence, the first thing to check after each run is the pressure in the SGs. The turbine control valve opening is adjusted manually due to the lack of turbine valve characteristic curve, so that the calculated secondary pressure matches with the corresponding one from the test data.

The first issue to be discussed in the following sections of this chapter is the thermal power ratio. Defining a realistic power ratio during the transient is one of the most challenging issues when performing transient runs. Then, some issues with the PRZ control systems found during the transient runs are discussed as well as the way they were tackled. Finally, the results of the best transient run, with the corresponding corrections of the model are presented.

5.1 Thermal Power Ratio

The current model is a "stand alone" thermohydraulic model and the time evolution of the thermal power level is not determined in a coupled neutron kinetic code. Consequently, the thermal power is user given input in a general table in the model. It is very important to give a table with realistic thermal power values as function of time in order to produce better results as possible. However, as it was underlined in the previous paragraphs, the thermal power is the most determining parameter, which has the strongest influence on the calculated results.

Three approaches were tested to derive the thermal power:

1. Set the thermal power ratio equal to the neutron flux/neutronic power (%) plant data. This is equivalent to assume linear interdependence between neutron flux and thermal power. The results are presented in figure 5.1.
2. Calculate the thermal power ratio by calculating the enthalpies of the feedwater and of the steam produced. Using the test data for pressure and feedwater, its enthalpy is calculated using water property tables. The enthalpy of the produced steam is calculated using steam properties table for quality $x = 1$ and the measured steam pressure values during the whole transient. Hence, the thermal power is calculated as:

$$Q_{tot} = \sum_{i=1}^{3} Q_{SG,i} = 3 \times \dot{m}_{fw}(h_{steam} - h_{fw})$$

   where the quantity $\dot{m}_{fw}(h_{steam} - h_{fw})$ is the thermal power produced by one SG. The thermal power along the transient is normalized with the time average of the calculated power using the above equation, from 0 to 338s. The calculated thermal power ratio is presented in figure 5.2.
3. Using the fact that $Q = \dot{m}c_p\Delta T$ it means that the thermal power ratio will be varying proportional to the temperature difference $\Delta T = T_{HL} - T_{CL}$ between the hot and cold leg. The temperature difference between the hot and cold leg is calculated using the corresponding test data for the whole transient, and is normalized with the average of the temperature differences from 0 to 338 s.The results are presented in figure 5.3.

Among the three fore-mentioned approaches the third one leads to better results. A quick look in figure 5.3 shows that the steam production/steam flow-rate behave in the same manner as the thermal power ratio. More thermal power translates into more steam and the opposite, as ones physical intuition dictates, which does not happen in the two previous approaches. In the first one, the thermal power ratio is tilted compared to the steam production during the intermediate steady-state. In the second half of the intermediate steady-state less thermal power produces the same amount of steam as in the first half with more thermal power. This is quite unphysical. In last part of the transient, after the power uprate the thermal power does not follow the steam production trend either. The second approach is incapable of reflecting the first seconds of the intermediate steady-state as well as the last part of the transient after the power increase.

As long as the thermal power ratio during the transient is set, then a power ratio table for 99 time entries (RELAP5 confinement) is built using the thermal power ratio from ΔT.

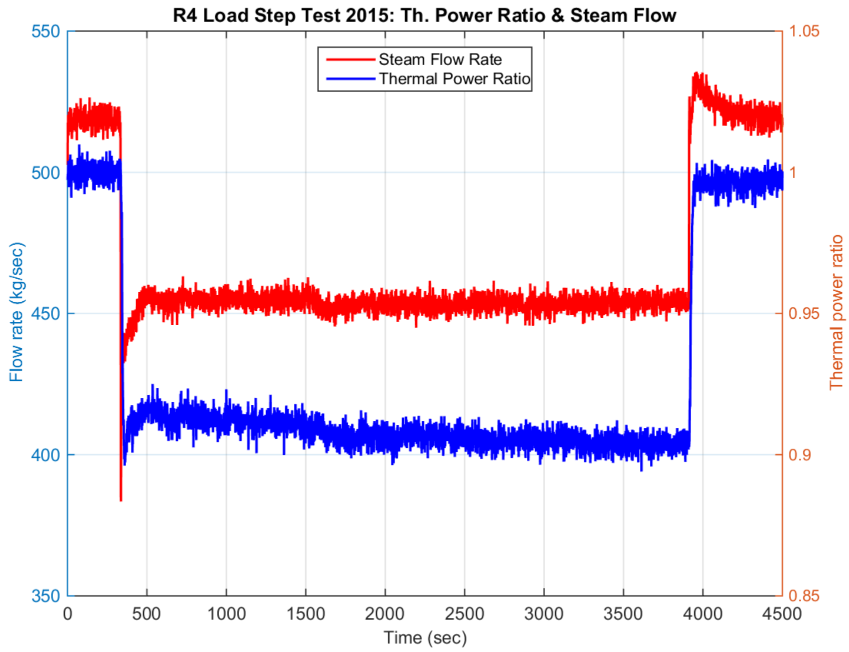

Figure 5.1: Steam flow-rate and thermal power ratio used in the calculation. The thermal power ratio is deduced from the neutron flux test data.

Figure 5.2: Steam flow-rate (left axis) and thermal power ratio used in the calculation. The thermal power ratio is calculated using the feedwater flow-rate and the enthalpies of the feedwater and of the steam.

Figure 5.3: Steam flow-rate (left axis) and thermal power ratio used in the calculation. The thermal power ratio is calculated based on the temperature difference between the hot and the cold leg.

5.2 Discrepancies in the PRZ

During the transient runs discrepancies in the calculated pressure and level in the PRZ have occurred (figures 5.5 and 5.6). In figure 5.5 it is observed that there are relatively high discrepancies during the power increase phase, roughly between 500 and 1500 s. During this time interval a high pressure overshoot takes place compared with the test data. Relatively high overshoots are observed in figure 5.6 between 500 and 1500 s as well. Likewise, in the second half of the intermediate steady-state and after that, the code cannot predict the measured level values as accurate as in the first phase of the transient. Not to mention that the calculated spraying control signal is half of the corresponding measured values during the power increase (figure 5.7).

Given that the PRZ pressure controllers have been checked and refined during the steady-state runs, the discrepancies in the spraying control signal indicate that the PRZ level controller may be a source of these discrepancies. The discrepancies in the calculated water level in the PRZ could originate due to overfeeding or improper feeding by the chemical and volume control system (CVCS), and thus, of the feeding flow (figure 5.4). A question may arise that what if the charging flow-rate or the spraying control signal would be equal to the corresponding test values? Would it eliminate the discrepancies in the calculated PRZ pressure and level?

In order to answer these questions, the code has been run for two different cases:

1. Manual spraying flow-rate and automatic charging flow-rate.
2. Manual charging flow-rate and automatic spraying flow-rate.

The second approach, the manual water charging of the primary side drastically improves all the results and consolidated the initial suspicion of poor documentation of the PRZ controllers, especially the of the PRZ level controller. Thus, it is decided to go along with manual charging water injection in the primary side for the rest of the transient calculations.

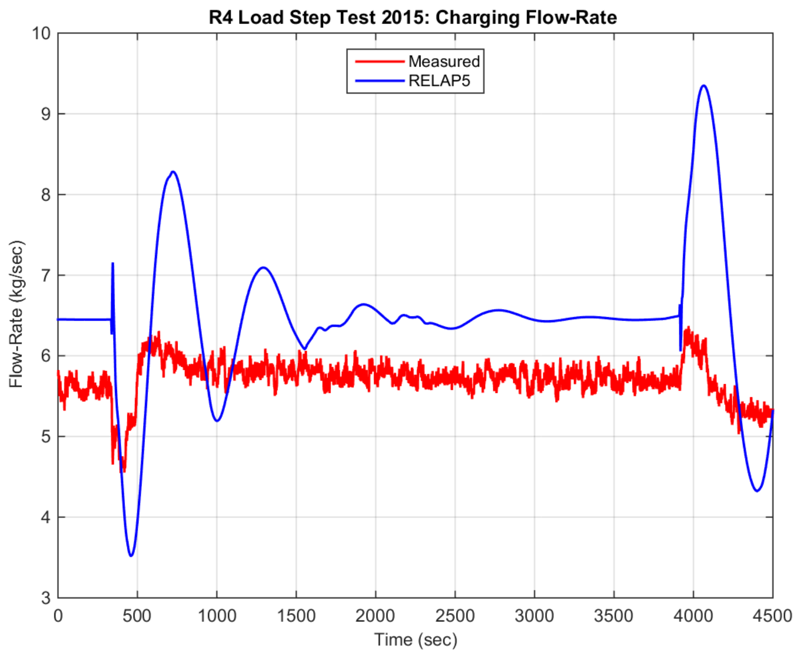

Figure 5.4: Charging flow-rate in the primary side. Discrepancies occur during the whole transient, however they intensify during the sharp thermal power decrease and increase.

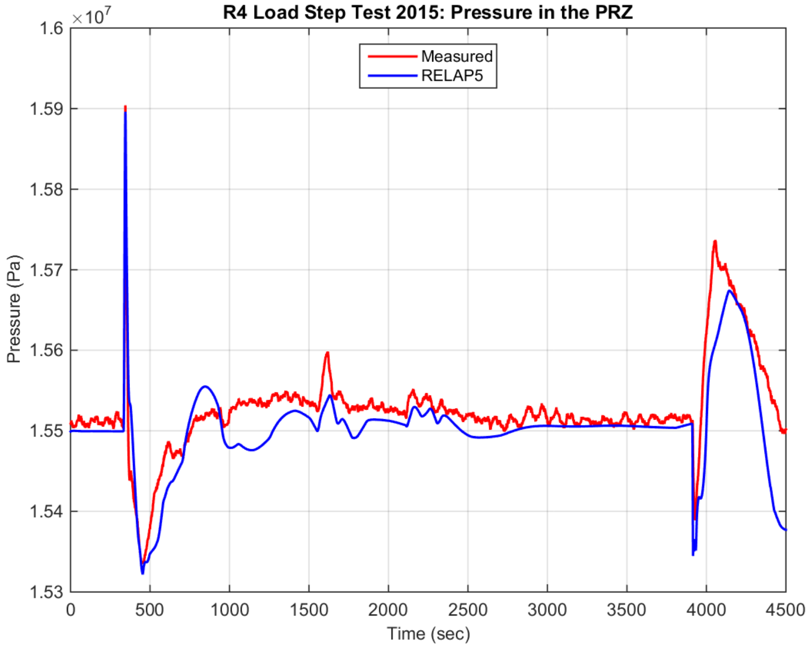

Figure 5.5: Pressure in the PRZ. Noticeable discrepancies occur between 500 and 1500 s as well as after 4000 s.

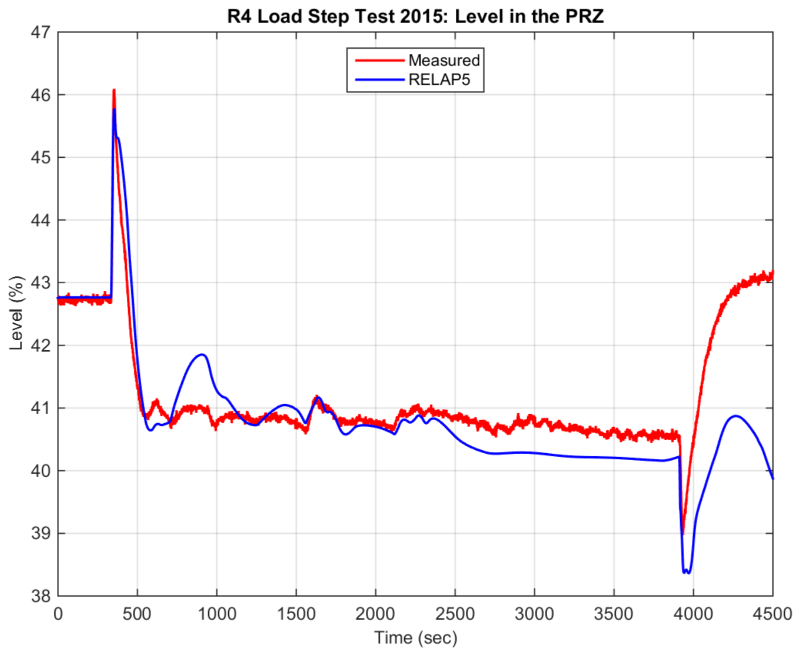

Figure 5.6: Water level in the PRZ. Noticeable discrepancies after 500 s.

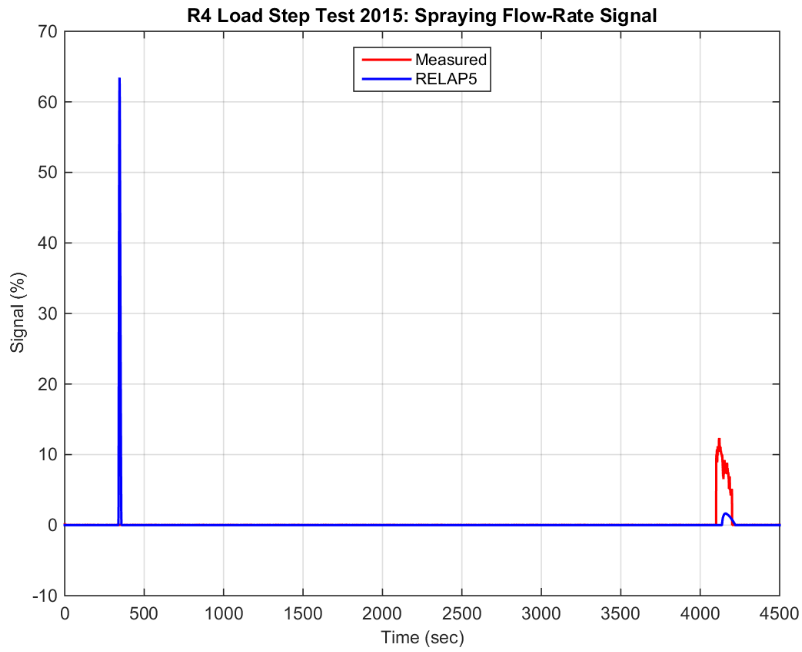

Figure 5.7: Output of spraying flow-rate controller. This control signal is translated into spraying flow-rate through the valve characteristic curve.

5.3 Transient Analysis Results

In the last series of transients runs the RELAP5 table of feedwater temperature is readjusted so as to capture the decrease of feedwater temperature during the intermediate steady-state.

Despite the fact that feedwater temperature changes roughly 4 K it seems that it affects the heat balance of the system and improves the calculated results when simulated.

It should also be noted that the length of the charging line is set equal with 10 m. Its previous value was 100 m an old estimate by the original developer of the code. The 100 m value for the length of the charging line seem to be exaggerated and that is the reason of its replacement with the most realistic 10 m value.

The results of the most successful transient run are presented in the following pages.

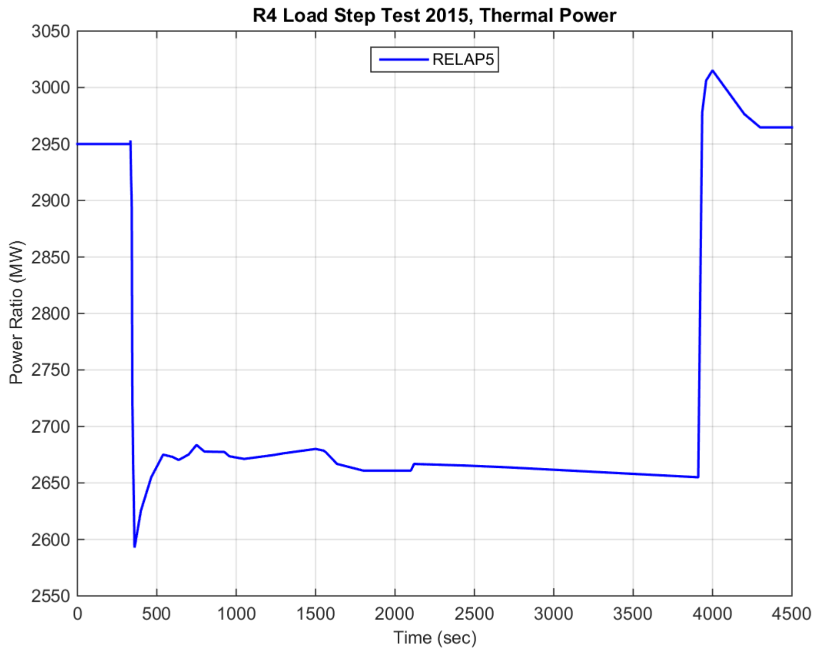

Figure 5.8: Thermal Power input for the transient runs.

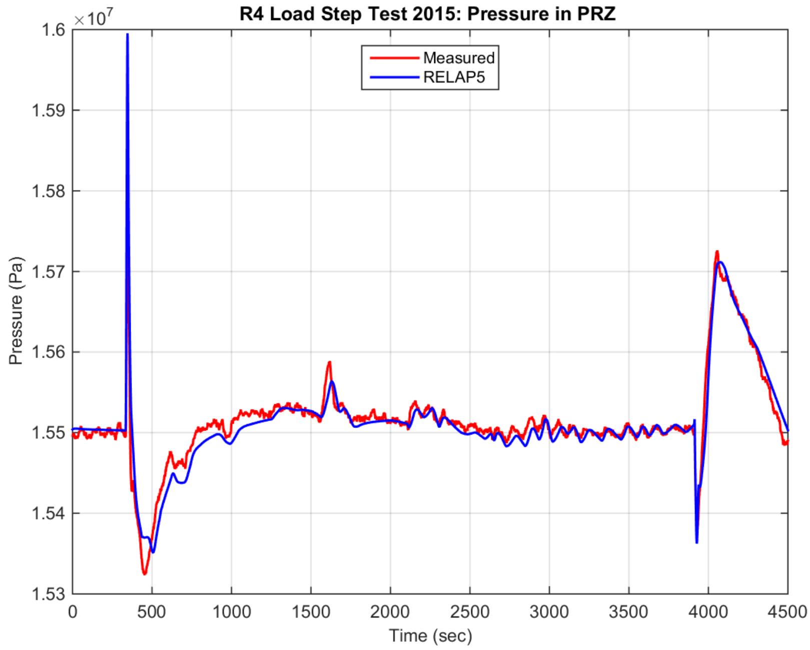

Figure 5.9: Pressure in the pressurizer.

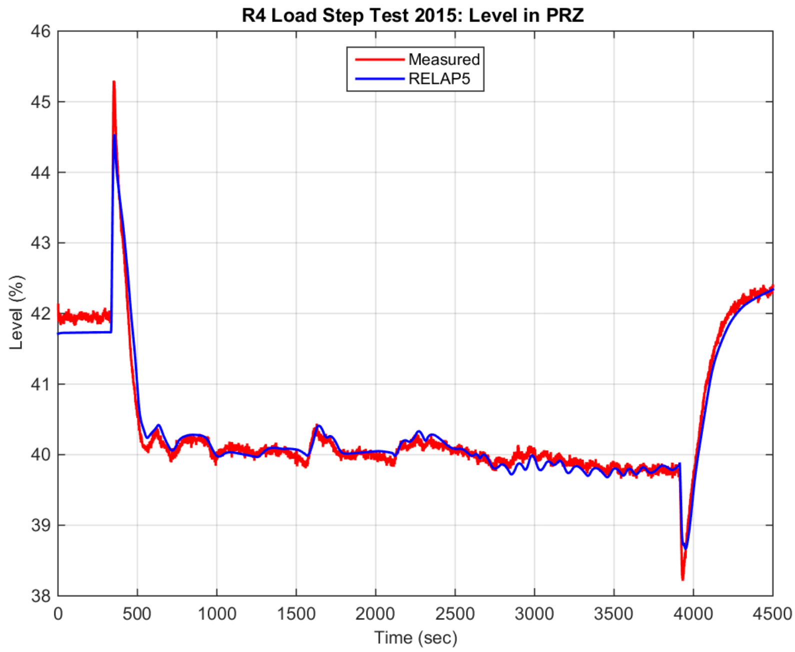

Figure 5.10: Level in the PRZ.

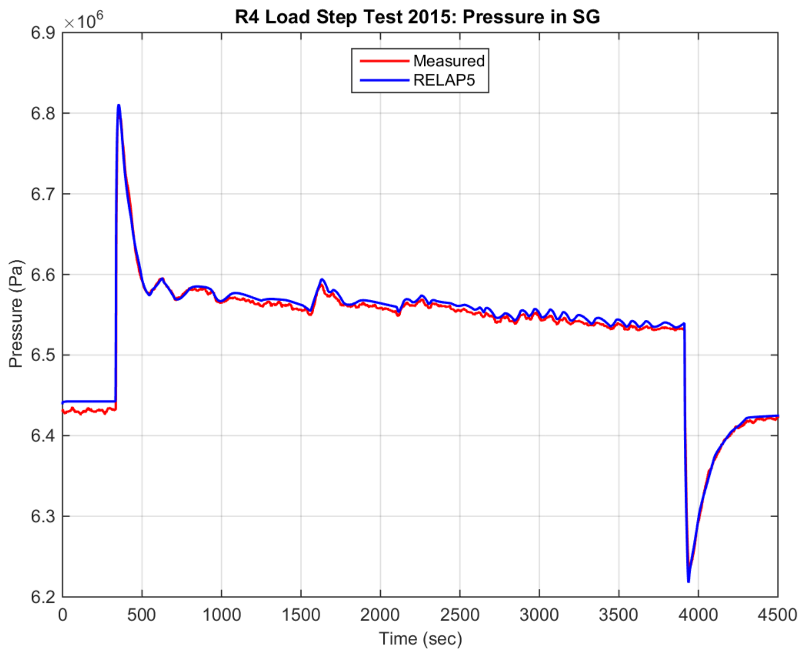

Figure 5.11: Pressure in the SG.

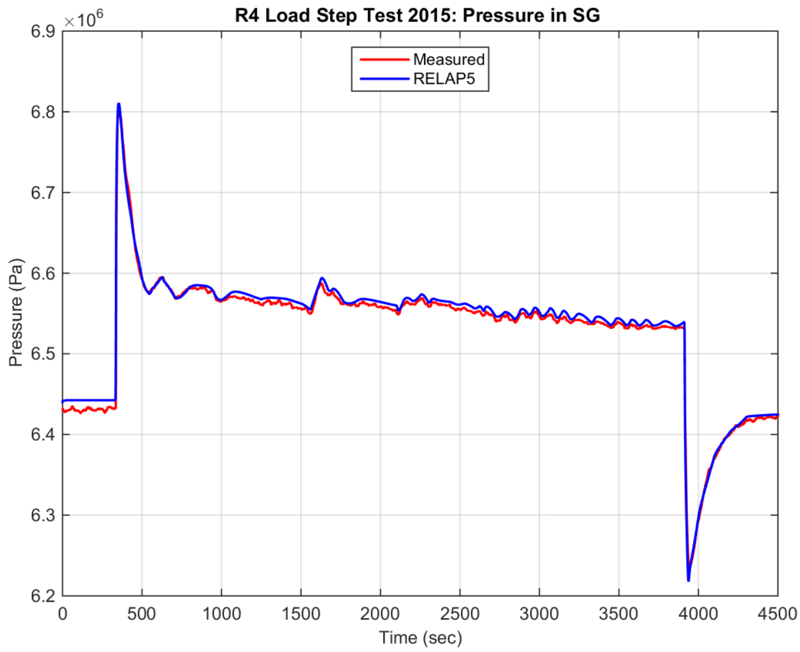

Figure 5.12: Level in the SG.

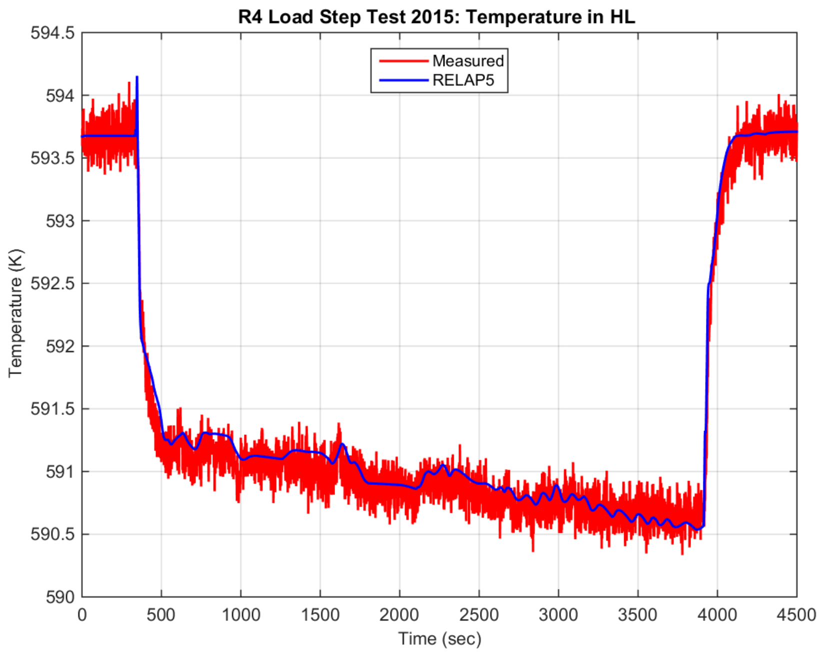

Figure 5.13: Temperature in hot leg.

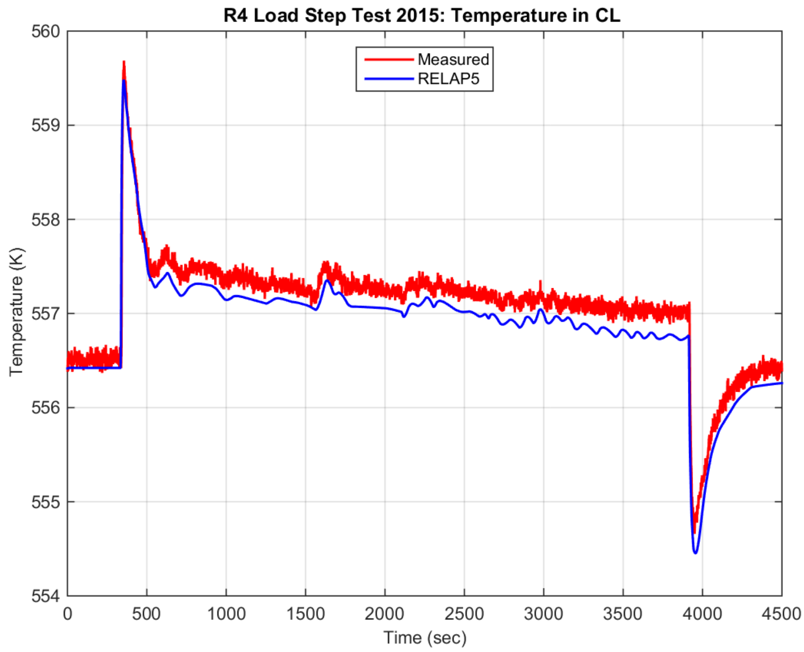

Figure 5.14: Temperature in cold leg.

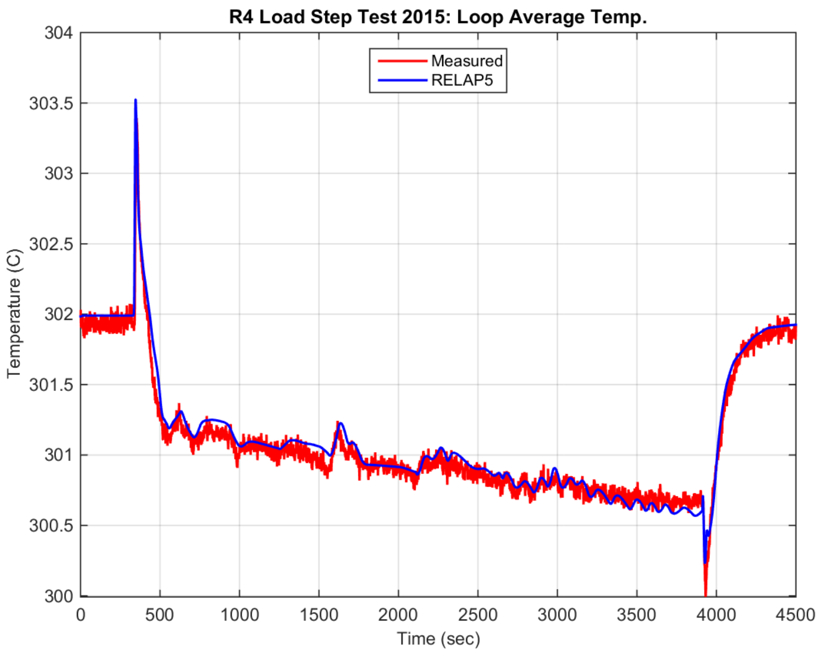

Figure 5.15: Loop average temperature.

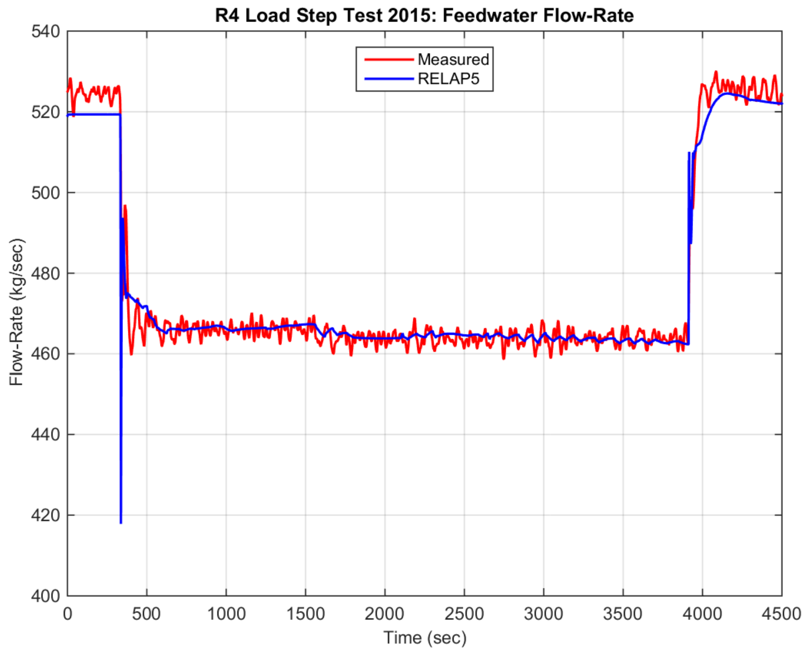

Figure 5.16: Feedwater flow-rate in the secondary side.

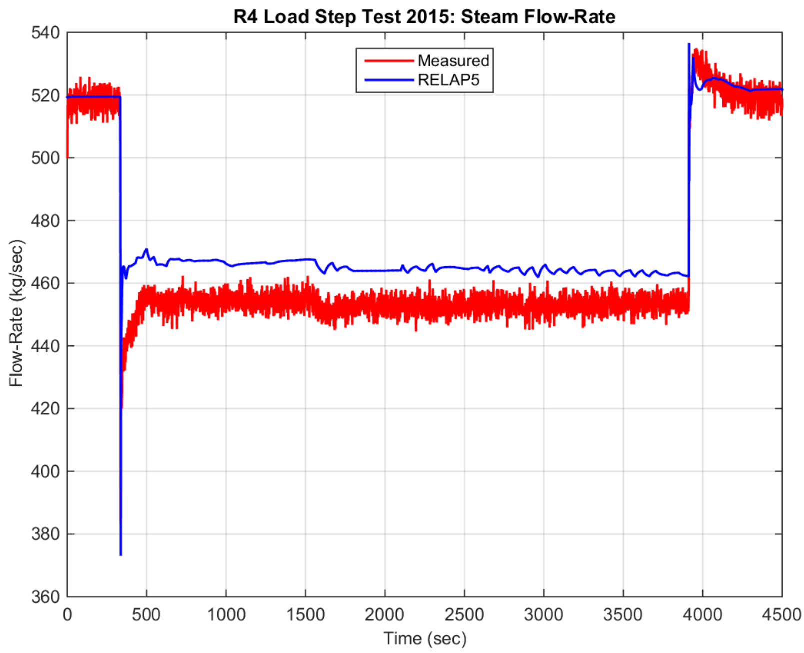

Figure 5.17: Steam flow-rate.

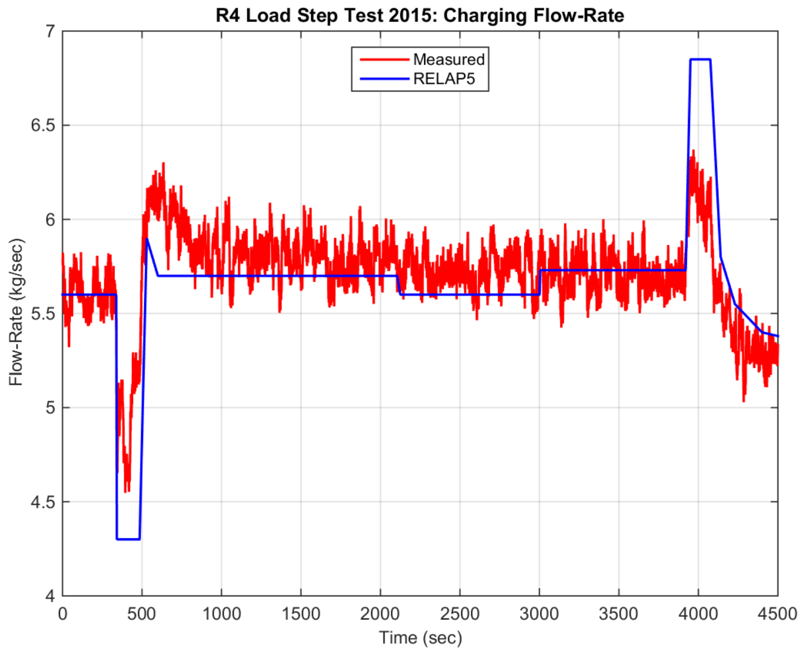

Figure 5.18: Charging flow-rate (given as boundary condition).

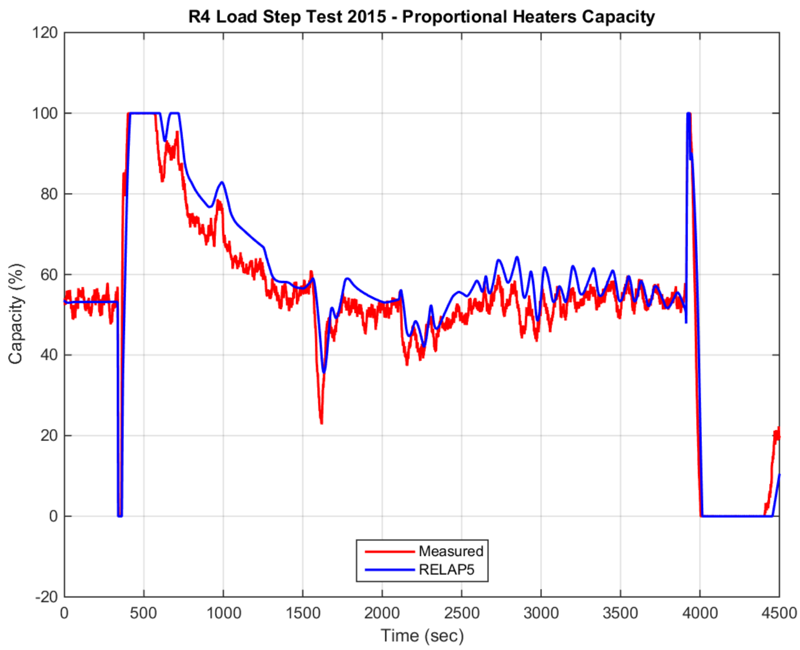

Figure 5.19: Proportional heaters capacity.

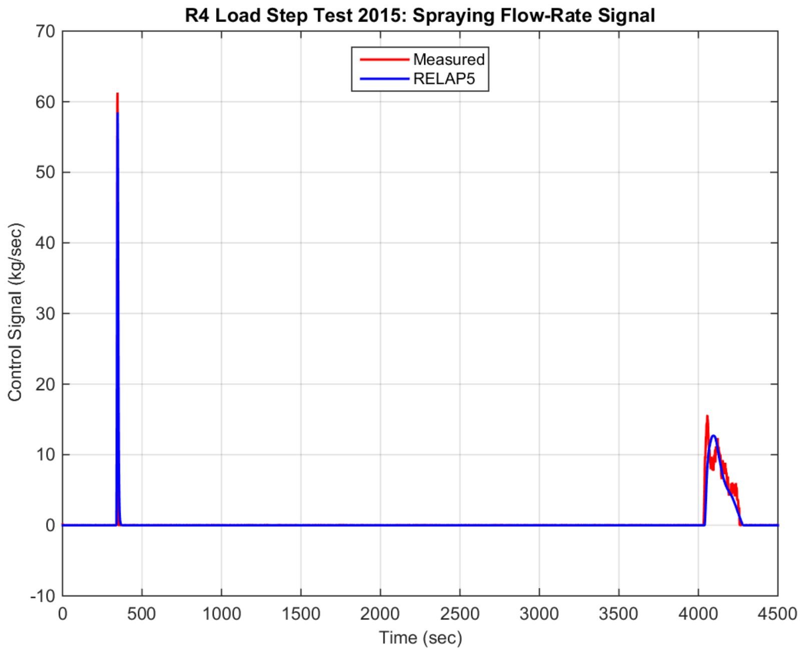

Figure 5.20: Spraying flow-rate signal.

The calculated values follow the trend of the test values and that almost all variables are predicted with very good precision. However, in some cases, like the feedwater flow (figure 5.16) overshooting is observed, not significant though, during the sharp power decrease and increase phases of the transient. However, a more thorough assessment of the accuracy of the code predictions is given by the FFTBM with signal mirroring in the following chapter.

5.4 Transient Analysis Concluding Remarks

The charging flow-rate is set as a boundary condition. This approach is followed in order to show that the results produced with charging flow set as boundary conditions are better than those when the charging flow is regulated automatically by the PRZ control systems. It is believed that improper modelling of the PRZ level controller mostly affects negatively the accuracy of the calculated results.

For manual charging flow-rate the calculated results seem to follow the trend of the corresponding test data and the vast majority of the variables are predicted with very small error, like the primary pressure (figure 5.9) and the loop average temperature (figure 5.15). Some others are predicted with a relatively higher error which are still between the acceptability limits. For instance, the steam flow- rates during the intermediate steady-state are predicted with relative error less than 5 %.

As for the spraying flow-rate signal concerned, it seems that despite the fact that the calculated results follow the trend of the test values, the peak of the spraying during the power decrease is not predicted as accurately as other variables, like the primary pressure. This happens because the calculated control signal decays slower than the actual one (not visible in figure 5.20). Again, this has to do with the PRZ controllers inadequate modelling.

However it should be noted that mass flow-rates in general are one of the most difficult values to be predicted by BE-codes.

6

Accuracy Quantification using Fast Fourier Transform Based Method (FFTBM)

Quite often BE-code users have to deal with the following questions [22]:

- How many simplifications can the model afford without deteriorating the prediction accuracy?
- What is the margin for necessary improvements in the model?
- How to perform an objective assessment of the model?

FFTBM is a method that deals with the above questions by depicting the discrepancies between the calculated and the experimental data in the frequency domain. It provides the means to assess the "goodness" of the method.

So far, FFTBM has been applied to primary side transients, especially for SB-LOCAs simulations in small-scaled facilities, secondary side transients as well as in burn-up calculations assessment.

6.1 FFTBM Outline

FFTBM is using Fast Fourier Transformation algorithm (FFT) in order to calculate the Discrete Fourier Transformation (DFT) of the experimental calculated signals. Thus, N samples from the experimental/calculated signals are needed. When FFT is used, in order for the sampling theorem to be fulfilled (the number of samples needed in order the experimental/calculated signal to be reliably represented by the sampled values) $N = 2^{m+1}, m = 8, 9, 10, 11$. Hence, the sampling frequency reads as:

$$\frac{1}{\tau} = f_s = 2f_{max} = \frac{N}{T_d} = \frac{2^{m+1}}{T_d},$$

where T_d is the duration of the sampled signal, τ the time interval between two successive samples and f_{max} the highest frequency component of the signal. The sampling theorem does not hold beyond f_{max}.

6.1.1 Average Amplitude

Average Amplitude AA is the basic measure used for FFTBM analysis. Supposing that the difference between the calculated $F_{cal}(t)$ signal and the experimental one

$F_{exp}(t)$ reads in the time domain as: $\Delta F = F_{cal}(t) - F_{exp}(t)$ then, the average amplitude AA is calculated as:

$$AA = \frac{\sum_{n=0}^{2^m} \tilde{\Delta} F(f_n)}{\sum_{n=0}^{2^m} \tilde{F}_{exp}(f_n)},$$

where $\tilde{\Delta} F(f_n)$ and $\tilde{F}_{exp}(f_n)$ the DFT of ΔF and F_{exp} as calculated by FFT algorithm respectively. AA can be interpreted as an integral measure that keeps track of the relative magnitude of the discrepancy between the experimental and calculated variable over the time history. Calculating the AA value of a variable of interest the following conclusions can be made for its prediction by the code:

- $AA \leq 0.3$ corresponds to very good variable prediction.
- $0.3 < AA \leq 0.5$ corresponds to good variable prediction.
- $0.5 < AA \leq 0.7$ corresponds to poor variable prediction.
- $AA > 0.7$ corresponds to very poor variable prediction.

This criterion refers to one variable. Usually, it is favorable to quantify the overall model accuracy based on a number of different variables N_{var}. Thus, the total average amplitude AA_{tot} for all of the variables of interest can be computed as:

$$AA_{tot} = \sum_{i=1}^{N_{var}} (w_f)_i (AA)_i$$

where $(w_f)_i$ the weighting factor of the $i-th$ variable of interest. The above criterion in this case is modified as:

- $AA_{tot} \leq 0.34$ corresponds to very good code prediction.
- $0.3 < AA_{tot} \leq 0.5$ corresponds to good code prediction.
- $0.5 < AA_{tot} \leq 0.7$ corresponds to poor code prediction.
- $AA_{tot} > 0.7$ corresponds to very poor code prediction.

There is a certain limit for the AA or AA_{tot} that should not be overwhelmed for experienced users, the so called "acceptability limit" $AA < 0.4$.

Those weighting factors are normalized, thus:

$$\sum_{i=1}^{N_{var}} (w_f)_i = 1$$

The weighting factor $(w_f)_i$ of the $i - th$ variable of interest is subsequently defined as:

$$(w_f)_i = \frac{(w_{exp})_i (w_{saf})_i (w_{norm})_i}{\sum_{i=1}^{N_{var}} (w_{exp})_i (w_{saf})_i (w_{norm})_i}$$

where $(w_{exp})_i$ accounts for the uncertainty due to the instrumentation or of the measurement method, $(w_{saf})_i$ the safety relevance of the variable, and $(w_{norm})_i$ the interrelation with the primary pressure since in a complex system like a nuclear reactor variables are not completely independent with each other. Primary pressure is a variable of significant importance therefore it is used as a benchmark for fixing $(w_{norm})_i$ values for different variables. Weighting factors $(w_{exp})_i$, $(w_{saf})_i$ and $(w_{norm})_i$ are usually referred to as experimental accuracy, safety relevance and primary pressure normalization respectively. These three weighting factors are not normalized usually. Their values are a subject of engineering judgment, which introduces a degree of arbitrariness, and as long as their values have been decided for a particular transient they should not be changed when comparing different codes/models results. FFTBM was first introduced for SB-LOCAs and the weighting factors were first estimated for this kind of transient, as shown in table 6.1.

Quantity	w_{exp}	w_{saf}	w_{norm}
Pressure Drops	0.7	0.7	0.5
Mass Inventories	0.8	0.9	0.9
Flow-Rates	0.5	0.8	0.5
Primary Pressure	1.0	1.0	1.0
Secondary Pressure	1.0	0.6	1.1
Fluid Temperatures	0.8	0.8	2.4
Clad Temperatures	0.9	1.0	1.2
Collapsed Levels	0.8	0.9	0.6
Core Power	0.8	0.8	0.5

Table 6.1: Weighting factors for different measured quantities (SB-LOCA) [8, 12, 22].

6.1.2 Additional Measures for Accuracy Quantification

Additional measures used in FFTBM analysis are the variable accuracy VA_i of the $i-th$ variable of interest, the minimal and maximal variable accuracy VA_{min} and VA_{max} respectively, as well as the number of discrepancies ND [8, 18].

Variable accuracy VA_i of the $i-th$ variable of interest shows what the total average amplitude AA_{tot} would be if the rest of the chosen variables all have the same weighting factor $(w_f)_i$ and average amplitude AA_i. Therefore it is designated as:

$$VA_i = (w_f)_i \cdot AA_i \cdot N_{var}$$

It should be mentioned that the criterion for AA is applicable for VA_i too. Minimal variable accuracy VA_{min} and maximal variable accuracy VA_{max} indicate the minimum and the maximum variable accuracy among the accuracy amplitudes $AA_i, i = 1, \ldots, N_{var}$ of the N_{var} chosen variables.

Consequently, they are defined as:

$$VA_{min} = max(VA_i), i = 1, \ldots, N_{var}$$

and

$$VA_{max} = min(VA_i), i = 1, \ldots, N_{var}$$

As it is mentioned before the acceptability limit is 0.4 and consequently $AA_{tot} < 0.4$. Hence, the number of discrepancies ND is equal with the number of variables for which $VA_i > 0.4$. It is obvious that $ND = 0$ when $VA_{min} < 0.4$. It should be mentioned that a prerequisite for the application of FFTBM is that the average amplitude of the primary pressure is $AA < 0.1$ due to the significant influence of this variable in the system.

6.2 Methodology for Code Accuracy Quantification

Initially, a qualitative assessment of the code results should take place to see whether the code predicts accurately the measured data and whether the calculated results follow the trend of the measured ones.

Then, the transient is divided in phenomenological windows for which the relevant thermal-hydraulic aspects (RTA) are identified (most important events/phenomena occurring). Variables that best describe the RTA are chosen. Then the weighting factors of the variables are set. The average amplitude AA of each chosen variable as well as the AA_{tot} can be calculated using the increasing time window approach.

In increasing time window approach the transient is divided in equal and successive time slots. Increasing time windows are then made by adding successive time slots so that the first time window corresponds to the first time slot, the second time window to the addition of the two first time slots etc. Hence, the last time window corresponds to the whole duration of the transient. AA_i for $i = 1, \ldots, N_{var}$ and AA_{tot} are calculated for each time window and plotted with time. This is the new increasing time window approach proposed in [8].

In the old increasing time window approach [22] the transient used to be partitioned in time slots equal with the duration of each phenomenological window. The time windows were constructed in the same manner as mentioned above, by adding successive time slots. Nonetheless, the new increasing time window approach allows to better track the evolution of AA_i or AA_{tot} with time, especially for transients with few phenomenological windows. In addition it reveals when the biggest discrepancies occur and their contribution both to variable and total accuracy.

In addition, the discrete calculated and discrete experimental signal are mirrored in the time domain in order to avoid an inherent weakness of the original FFTBM method that produced unphysical AA results [10]. AA (AA_i or AA_{tot}) should increase with increasing time window, since it is an integral discrepancy measure throughout the increasing time window interval. Consequently as time window increases, addition of discrepancies of the newly added time slots occur, which is why AA should monotonically increase. However this does not happen when the last and the first point of the discrete signal differ significantly. FFT multiplies the discrete signal so as to create a periodic infinite signal. As a result, any difference between the first sample of each period with the last sample of the previous period increases the frequency content of AA, distorting it significantly.

6.3 FFTBM Analysis

The quantitative analysis is described in the *Transient Analysis (2) - Transient Results* chapter. The main conclusion of the qualitative analysis is that overall the calculated results are in very good agreement with the corresponding experimental values.

Then, FFTBM with signal mirroring is applied for the quantification of the goodness of the model used mainly through average amplitude AA.

The transient is partitioned in five phenomenological windows:

1. Initial Steady-State, $0 - 338\ s$
2. Power Decrease, $338 - 500\ s$
3. Intermediate Steady-State, $500 - 3914\ s$
4. Power Increase, $3914 - 4300\ s$
5. Stabilizing in the Initial Steady-State, $4300 - 4500\ s$

A number of 25 variables descriptive of the most important RTA were chosen for the assessment, those that appear as inputs or outputs in the PRZ level and pressure controllers as well as in SG level controller (table 6.2).

The safety and experimental weighting factors used are the same as the ones used for the SB-LOCA transient. The normalised factors are chosen as the average amplitude for each variable divided by the average amplitude of the primary pressure.

For the FFTBM analysis JSI FFTBM Add-in 2007 is used. It is an Excel-2007 add-in developed by Jožef Stefan Institute in Ljubljana by Dr. Andrej Prošek. The user should tabulate the experimental as long as the calculated data. The options provided by the add-in is FFTBM with or without signal mirroring, Safety Analysis Report (SAR) analysis and plotting of the experimental versus the calculated data.

6.4 FFTBM Results

The results for the biggest time window $0-4500\ s$ are representative of the variables trends during the whole transient and they are presented in table 6.2. From figure 6.1 it can be seen that the primary pressure criterion $AA < 0.1$.

The evolution of total average accuracy AA_{tot} is depicted in figure 6.12. It can be seen that the total average accuracy is below the acceptability limit and that the overall predictions of the code are good.

The number of discrepancies (variables with $VA > 0.4$) in the $0 - 4500\ s$ time window is equal to 5, which is due to the steam flow-rates, the spraying flow-rate signal and the proportional heaters capacity.

However, from the figures and from the AA - VA data in table 6.2 it can be seen that the spraying flow-rate signal (figure 6.11) is the variable with the most deleterious influence in total average accuracy. Its AA and VA are well above the acceptability limit.

The second variable that negatively influences the code accuracy is the proportional heaters capacity (figure 6.10) and last, the steam flow-rates figure(6.9). The behaviour of spraying and of the proportional heaters substantiates the suspicions for the controllers modelling.

Seventeen variables have $AA \leq 0.1$. Hence their prediction is excellent and it is very noticeable that among those variables the most important system variables are included. Namely, the primary pressure, the secondary pressure, the levels of the SGs and of the PRZ, and all temperatures.

$Variable$	$Weightingfactors$			$0 - 4500s$	
	w_{exp}	w_{saf}	w_{norm}	AA	VA
Primary Pressure	1.0	1.0	1.0	0.02	0.006
Level in PRZ	0.8	0.9	4.1	0.09	0.1
Pressure in SG-1	1.0	0.6	1.1	0.02	0.004
Pressure in SG-2	1.0	0.6	1.3	0.03	0.005
Pressure in SG-3	1.0	0.6	1.2	0.03	0.004
Level in SG-1	0.8	0.9	4.2	0.09	0.07
Level in SG-2	0.8	0.9	4.5	0.10	0.08
Level in SG-3	0.8	0.9	4.3	0.10	0.08
Hot Leg Temp. in Loop 1	0.8	0.8	0.3	0.02	0.001
Hot Leg Temp. in Loop 2	0.8	0.8	0.4	0.02	0.001
Hot Leg Temp. in Loop 3	0.8	0.8	0.4	0.02	0.001
Cold Leg Temp. in Loop 1	0.8	0.8	11.7	0.01	0.02
Cold Leg Temp. in Loop 2	0.8	0.8	11.1	0.01	0.02
Cold Leg Temp. in Loop 3	0.8	0.8	11.8	0.01	0.02
Average Temp. in Loop 1	0.8	0.8	0.3	0.008	0.0004
Average Temp. in Loop 2	0.8	0.8	0.4	0.008	0.0004
Average Temp. in Loop 3	0.8	0.8	0.4	0.008	0.0004
Feedwater Flow in SG-1	0.5	0.8	11.7	0.26	0.30
Feedwater Flow in SG-2	0.5	0.8	11.1	0.25	0.27
Feedwater Flow in SG-3	0.5	0.8	11.8	0.27	0.31
Spraying Control Signal	0.5	0.8	43.1	0.97	4.15
Prop. Heaters Capacity	0.8	0.8	19.7	0.44	1.39
Steam Line - 1 Flow	0.5	0.8	14.1	0.32	0.44
Steam Line - 2 Flow	0.5	0.8	16.1	0.36	0.58
Steam Line - 3 Flow	0.5	0.8	14.9	0.33	0.50
Total				0.33	

Table 6.2: FFTBM analysis variables, weighting factors and results for the $0-4500$ s interval

From the total accuracy figure (figure 6.12) and from the spraying flow-rate signal figure (figure6.11) it can be deduced that it is mostly the discrepancies during the first spraying period that contributes negatively to the accuracy of this variable and to the total accuracy. In other words the big jump in AA_{tot} diagram is caused by the jump occurring in the AA of the spraying flow-rate signal. In the same trend the discrepancies of every variable during the power decrease phase are greater than in the rest of the transient, especially compared to the discrepancies occurring during the power increase phase. It seems that the modeled control systems are initially "shocked" due to the power decrease but then they manage to compensate the transient.

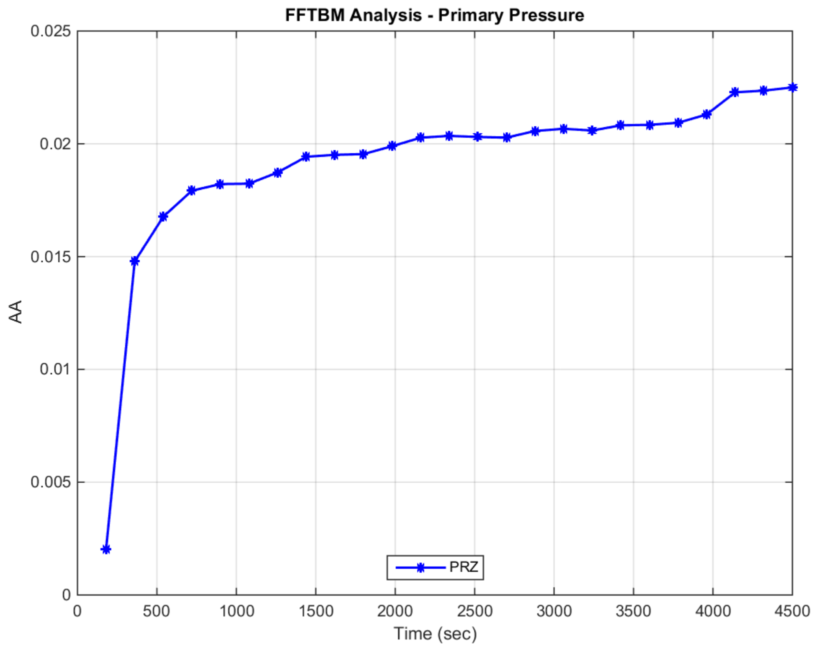

Figure 6.1: Average amplitude of the primary pressure.

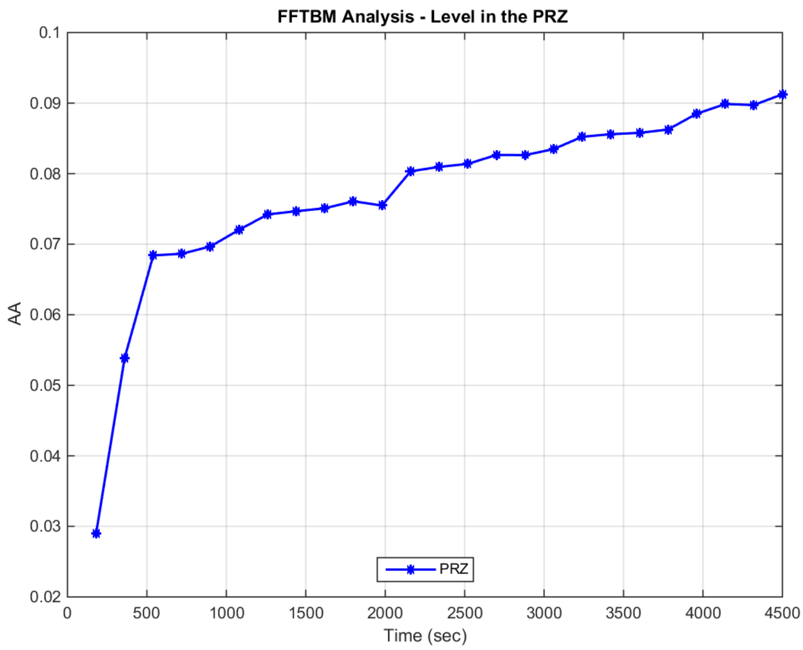

Figure 6.2: Average amplitude of level in the PRZ.

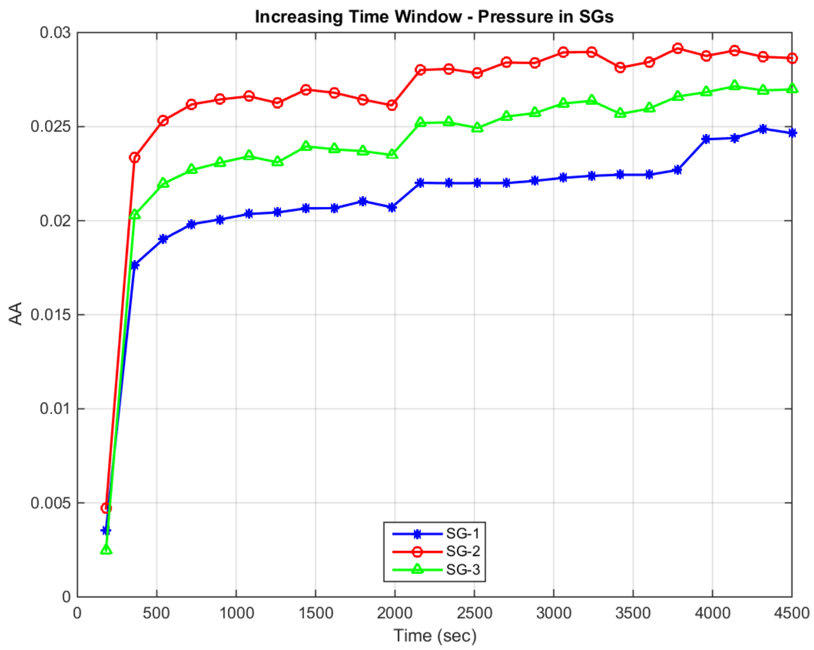

Figure 6.3: Average amplitudes of the pressure in the SGs.

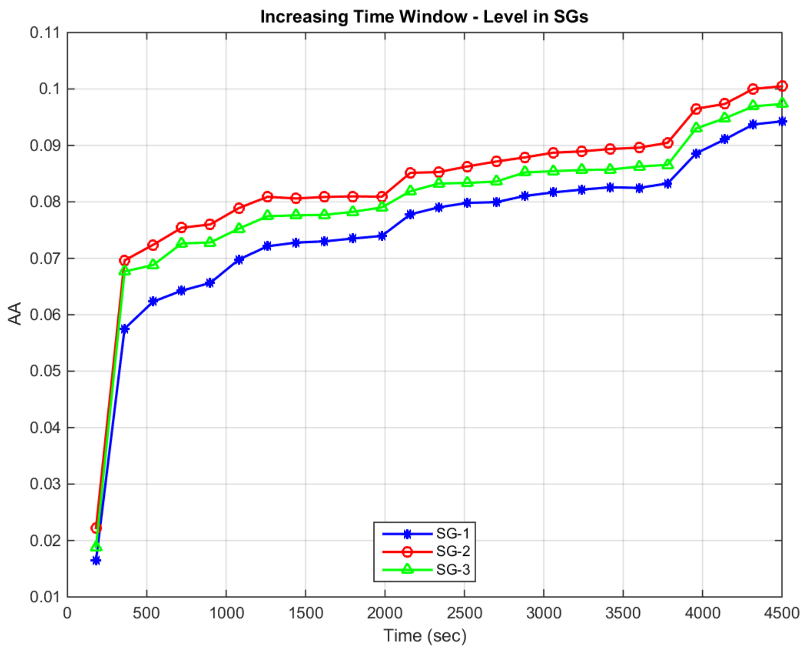

Figure 6.4: Average amplitudes of the levels in the SGs.

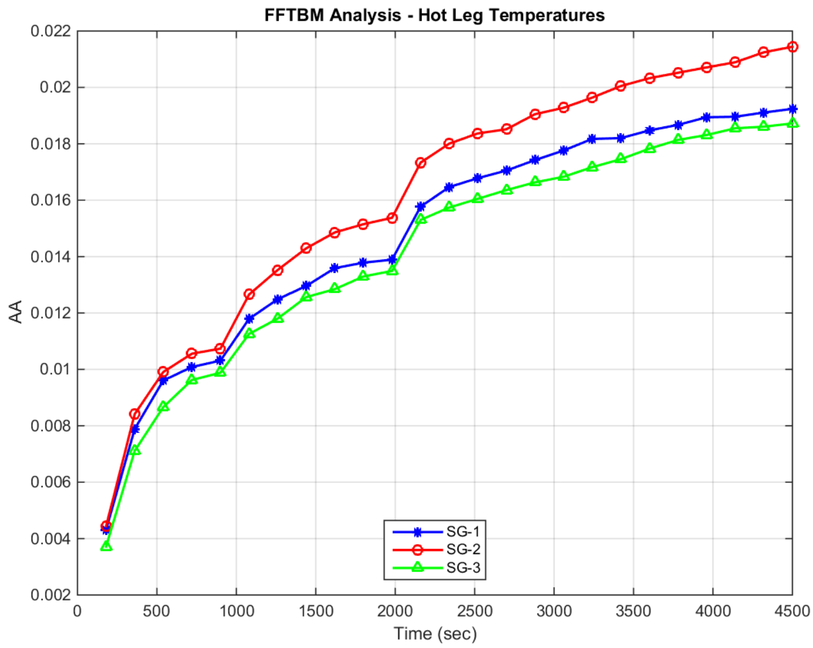

Figure 6.5: Average amplitudes of the hot leg temperatures in the SGs.

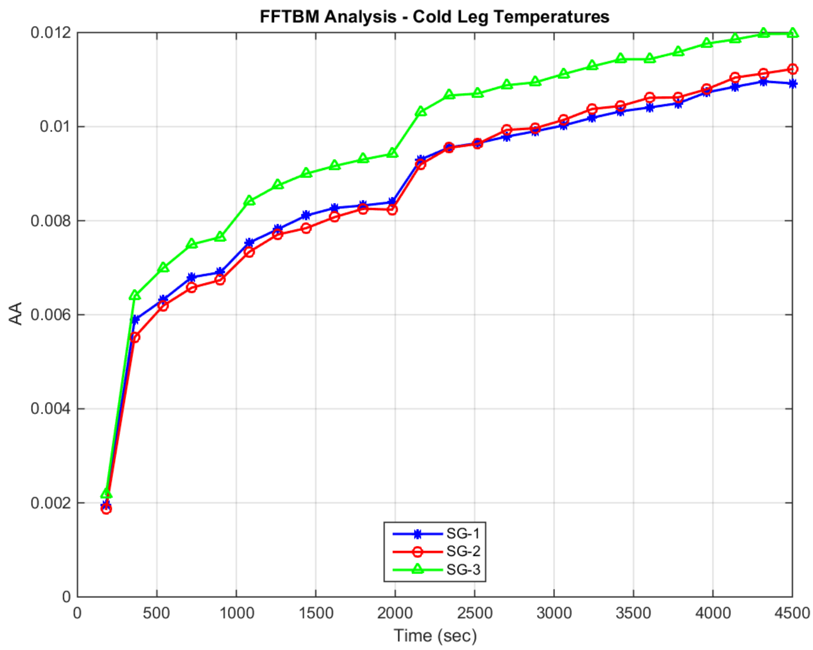

Figure 6.6: Average amplitudes of the cold leg temperatures in the SGs.

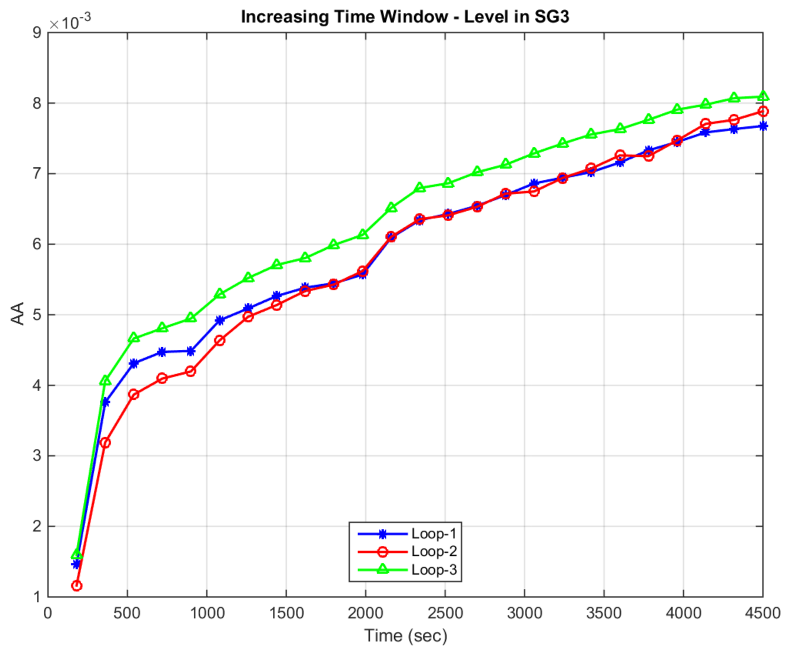

Figure 6.7: Average amplitudes of the average loop temperatures.

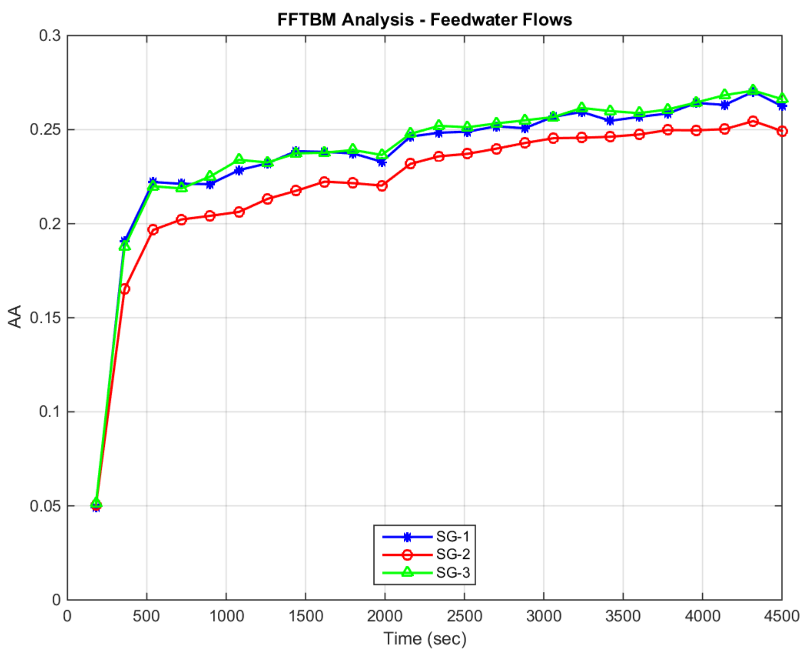

Figure 6.8: Average amplitudes of the feedwater flow-rates in the SGs.

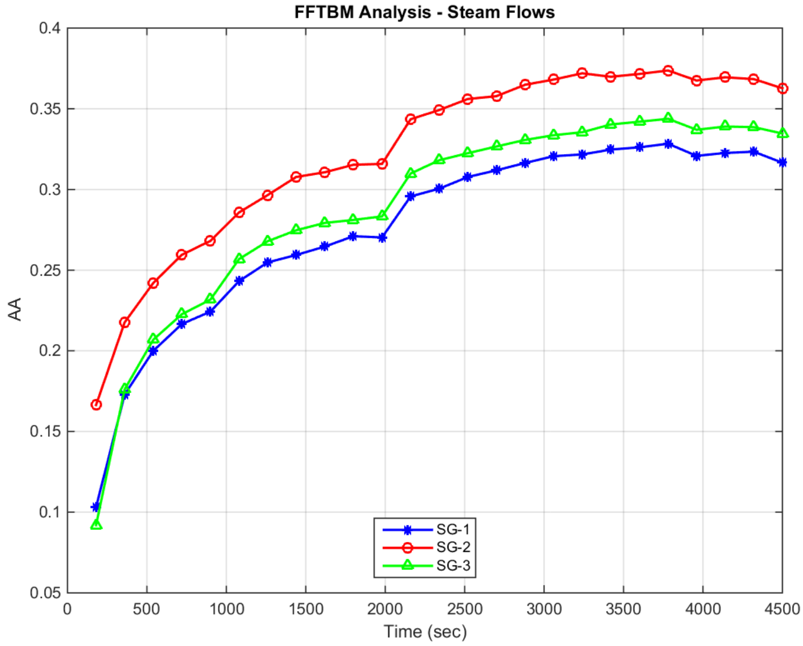

Figure 6.9: Average amplitudes of the steam flow-rates in the SGs.

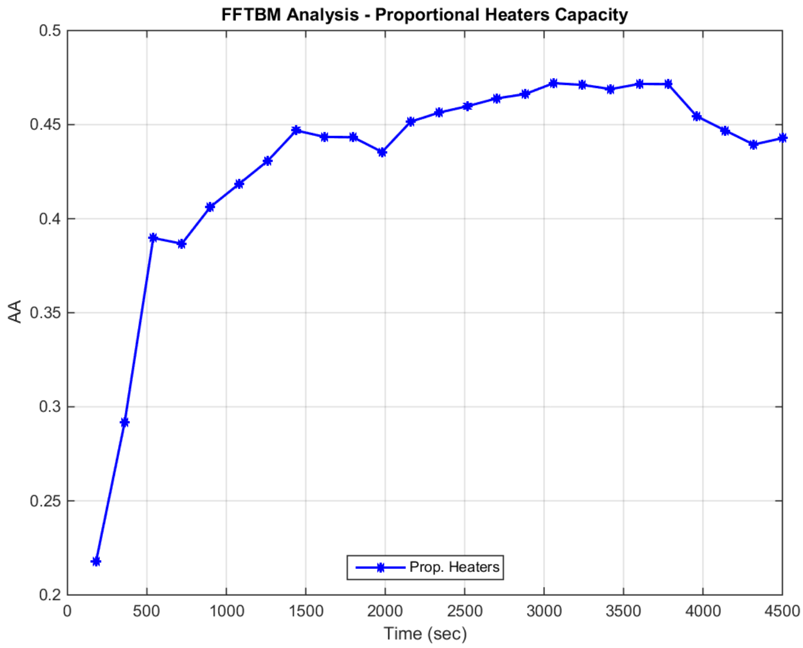

Figure 6.10: Average amplitude of the proportional heaters capacity.

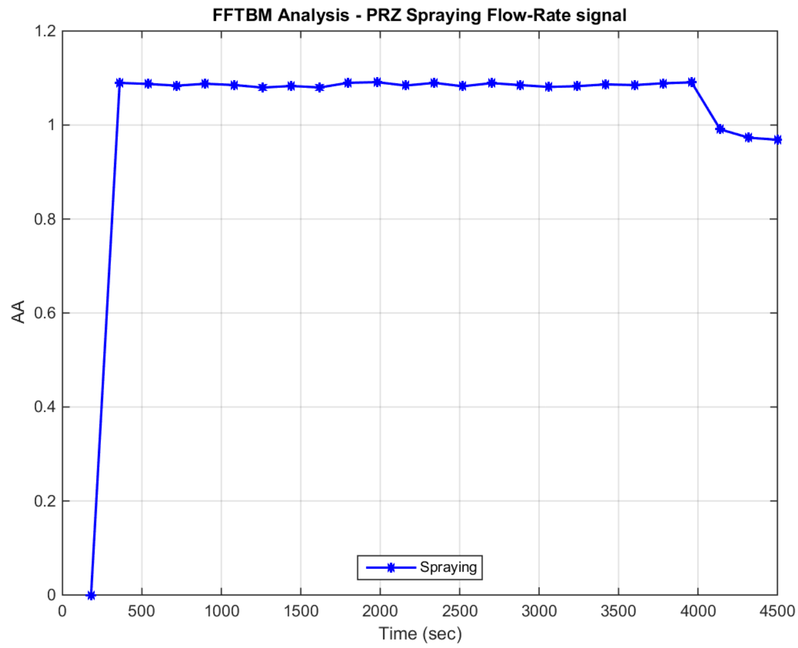

Figure 6.11: Average amplitude of the spraying flow-rate signal.

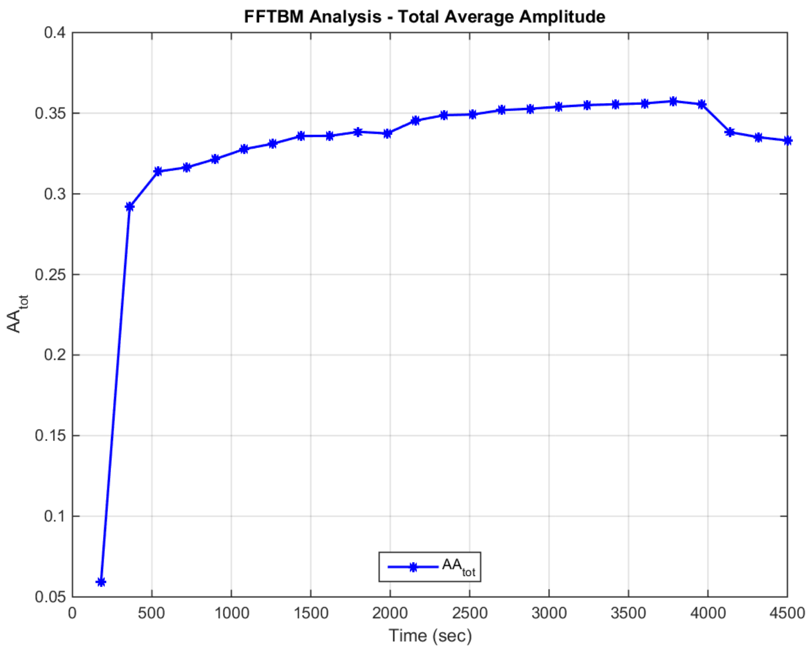

Figure 6.12: Total average amplitude.

6.5 FFTBM Analysis Concluding Remarks

In general, on the basis of the FFTBM analysis it can be concluded that the code predictions of the most important parameters, like the primary and secondary pressure are excellent.

Figure 6.12 indicates that the quality of overall code predictions are in the range of good agreement. Yet, there is a margin for further improvement by re-examination and possible re-adjustment of the modeled PRZ controllers, especially the PRZ level controller.

7

Conclusion

This chapter presents the most important results of the previous analysis and a recommendation for future work is given.

7.1 Summary - Main Conclusions

The main purpose of the Load Step Test is to check the ability of the control systems to handle the perturbations without triggering any safety or protection systems. This should also be reflected in the simulation of the Load Step Test by the RELAP5 model of Ringhals 4, which is successful.

The first step for the simulation of the transient is that the code is able to achieve a steady-state close to one of the real reactor. The code reaches a steady-state after 6000 s and the steady-state values of the most important variables predict the corresponding test data values.

Thermal power level throughout the transient is the most important parameter affecting the calculated results. Deriving it from the temperature difference between the hot and the cold legs is the most reliable way.

Investigation of the calculated PRZ level discrepancies revealed that the cause lied in the inappropriate modeling of the CVCS system which affected the feeding flow of the PRZ from the surge line as well as the spraying flow. Hence, the remaining transient calculations were run with the primary side charging flowrate given as a boundary condition.

The FFTBM analysis shows the overall reliability of the code predictions. The predictions of the most important variables, 20 out of the 25 chosen variables, can be labeled as very good. The predictions for the spraying control signal and the proportional heaters are not satisfactory. The last two indicate that the modelling of the PRZ controllers has to be improved. Thus, additional data like spraying valve characteristics will be needed.

7.2 Proposals for Future Work

The work presented above revealed the inappropriate modelling of the PRZ level control system (CVCS). Consequently, the most important recommendation for future work is the re-examination of the PRZ control system because this will contribute to the improvement of the results.

The weighting factors that were set for the FFTBM analysis of the Load Step Test are presented in table 6.2. As it is mentioned in a previous chapter, the weighting factors are set for different transient types and their values are a subject of engineering judgement. It would be useful to further if more appropriate weighting factors could be set.

Furthermore, development of a PARCS neutron kinetic model for Ringhals 4 which will be coupled with the existing RELAP5 model will pave the way for a more complete and integrated neutronic-thermalhydraulic model of Ringhals 4, increasing the model fidelity and ultimating the ability of transient predictions.

Another option for future work is the conversion of RELAP5/MOD3.3 model of Ringhals 4 to TRACE, which is a new and more user-friendly code compared to RELAP5.

Bibliography

[1] Information Systems Laboratory Inc., *RELAP5/MOD3.3 Code Manual, Volume II: User's Guide and Input Requirements*, 2010, US Nuclear Regulatory Commission.

[2] Information Systems Laboratory Inc., *RELAP5/MOD3.3 Code Manual Volume V: User's Guidelines*, 2010, US Nuclear Regulatory Commission.

[3] *Ringhals 4-Frej Project-Software Settings.*

[4] J. Bánáti, A. Stathis *Validation of the RELAP5 Model of RINGHALS 4 against a Load Step Test at Uprated Power"*, Chalmers University of Technology, Department of Applied Physics, Division of Nuclear Engineering, 2015.

[5] J. Bánáti, *Technical Description of the RELAP5 Model forRINGHALS 4 NPP*, Chalmers University of Technology, Department of Applied Physics, Division of Nuclear Engineering, 2013.

[6] A. Agung, J. Bánáti, M. Stålek, C. Demaziere, *Validation of PARCS/RELAP5 coupled codes against a load rejection transient at the Ringhals-3 NPP*, Nuclear Engineering and Design, 2013, vol.257, p.31-44.

[7] J. Bánáti, *Validation of the RELAP5 Model of RINGHALS 4 against the 2011-12-14 ± 10 % Load Step Test"*, Chalmers University of Technology, Department of Applied Physics, Division of Nuclear Engineering, 2013.

[8] A. Prošek, B. Mavko", *Quantitative Code Assessment with Fast Fourier Transform Based Method improved by Signal Mirroring*, Nuclear Regulatory Commission, NUREG/IA-0220, December 2009.

[9] H. Glaeser *CSNI Integral Test Facility Matrices for validation of Best Estimate Thermal-Hydraulic Computer Codes*, THICKET 2008-Session III-Paper 04.

[10] A. Prošek, M. Leskovar, B. Mavko, *Quantitative Assessment with improved fast Fourier transformed based method by signal mirroring*, Nuclear Engineering and Design, 2008, vol.238, p.2668-2677.

[11] A. Petruzzi, F. D'Auria, *Thermal Hydraulic System codes in Nuclear Reactor Safety and Qualification Procedures*, Science and Technology of Nuclear Installations, 2008.

[12] A. Prošek, *JFI FFTBM Add-in 2007 Users Manual*, Jožef Stefan Institute, Ljubljana, December 2007.

[13] M. J. Moran, H. N. Shapiro, *Fundamentals of Engineering Thermodynamics, 5th Edition, SI Units*, John Wiley Sons, 2006.

[14] A.Prošek, F. D'Auria, D. J. Richards, B. Mavko, *Quantitative assessment of thermal-hydraulic codes used for heavy water reactor calculations*, Nuclear Engineering and Design, 2006, vol.236, p.295-308.

[15] A.Prošek, *FFTBM and Primary Pressure Acceptance Criterion*, Nuclear Energy for New Europe International Conference-2004, 2004, Portoro, Slovenija.

[16] J. Lillington, *The future of Nuclear Power*, Elsevier, 2004.

[17] M. Schleicher, F. Blasinger, *Control Engineering, a Guide for Beginners, 3rd Edition*, JUMO GmbH Co. KG, 2003.

[18] A. Prošek, B. Mavko, *A tool for Quantitative assessment of code calculations with an improved fast Fourier transform based method*, Elektrotehniški vestnik, 2003.

[19] J. Wilkie, M. Johnson, R. Katebi, *Control Engineering, an Introductory Course*, Palgrave Macmillan, 2002.

[20] A.Papaioannou, *Fluid Mechanics, Vol. 2, (in Greek)*, Korali, 2002.

[21] A.Prošek, *Lessons Learned from Accuracy Assessment of IAEA-SPE-4 Experiment Predictions, Nuclear Energy for New Europe International Conference-2002*, 2002, Kranjska Gora, Slovenija.

[22] A. Prošek, F. D'Auria, B. Mavko, *Review of Quantitative Accuracy Assessment with Fast Fourier Transform Based Method (FFTBM)*, Nuclear Engineering and Design, 2002, vol.217, p.179-206.

[23] N. E. Todreas, M. S. Kazimi, *Nuclear Systems II, Elements of Thermal Hydraulic Design*, Taylor Francis, 2001.

[24] B. Preshagen, *Light Water Reactor Safety*, Pergamon Press, 1998.

[25] B. Mavko, A. Prošek, F. D'Auria, *Determination of code accuracy in predicting small break LOCA experiment*, Nuclear Engineering and Design, 1997, vol.120.

[26] N. E. Todreas, M. S. Kazimi, *Nuclear Systems I, Thermal Hydraulic Fundamentals*, Taylor Francis, 1993.

[27] S. N. Aksan, F. D'Auria, H. Städke, *User Effects on the thermal-hydraulic transient system code calculations*, Nuclear Engineering and Design, 1993, vol.245, p.159-174.

[28] S. N. Aksan, F. D'Auria, H. Städke, *CSNI code validation matrix of thermo-hydraulic codes for LWR LOCA and transients*, Committee on the safety of nuclear installations, OECD Nuclear Energy Agency, 1987.

[29] Westinghouse Electric Corporation, Water Reactor Divisions, *The Westinghouse Pressurized Water Reactor Nuclear Power Plant*, 1984.

[30] IAEA country nuclear profiles: Sweden, 2015 edition,
`http://www-pub.iaea.org/MTCD/Publications/PDF/CNPP2015_CD/countryprofiles/Sweden/Sweden.htm`

[31] PWR diagram,
`http://www.edusolution.com/current_issues/nuclear/nuclear3`

[32] IAEA country nuclear profiles: Sweden, 2015 edition,
`http://www-pub.iaea.org/MTCD/Publications/PDF/CNPP2015_CD/countryprofiles/Sweden/Sweden.htm`